Urban Climate 37 (2021) 100851

Contents lists available at ScienceDirect

Urban Climate

journal homepage: www.elsevier.com/locate/uclim

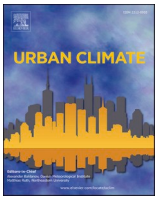

Traffic accidents and delays present contrasting pictures of traffic resilience to coastal flooding in the San Francisco Bay Area, USA

Indraneel Kasmalkar [a,*], Jenny Suckale [a,b,c]

[a] Institute for Computational and Mathematical Engineering, Stanford University, Stanford, California, USA
[b] Department of Geophysics, Stanford University, Stanford, California, USA
[c] Department of Civil and Environmental Engineering, Stanford University, Stanford, California, USA

ARTICLE INFO

Keywords:
Coastal flooding
Transportation
Resilience
Traffic accidents
Sea level rise

ABSTRACT

Climate change is intensifying coastal floods and increasing the risks of traffic disruption in low-lying, coastal communities. Efforts to understand the differential impacts of traffic disruption on communities have led to the concept of traffic resilience which captures the degree to which a traffic system can recover from disruption. Existing proxies of traffic resilience are focused on quantifying travel time delays but lack the important dimension of road safety. In this study, we quantify traffic resilience in terms of the change in non-highway car and pedestrian accident rates during the 5–10 am period as a result of coastal flooding in the San Francisco Bay Area for the 2020–2040 period. We use a regional traffic model to simulate traffic patterns under a range of coastal flood water levels. We use regressions that relate traffic volumes to historical accident rates to estimate accidents rates in the presence of flooding. Our results show that the flooding of highways forces commuters onto local roads passing through residential communities, causing a spike in accident rates. Unlike delays which increase sharply at the higher water levels considered in this study, we project that region-wide peak-hour accident rates may increase substantially at lower water levels.

1. Introduction

A rising sea level and intensifying storms are causing more frequent and more intense coastal flood events, impacting communities in low-lying coastal regions (Wong et al., 2014). The disruptions associated with coastal flooding come at a time of unprecedented population growth and wide-spread urbanization, especially in coastal regions (Neumann et al., 2015; Merkens et al., 2016; United Nations Population Division, 2018). As a result, coastal flooding can trigger spatially extensive impacts on dense, urban regions by disrupting highly interdependent and interconnected urban systems such as transportation (Kasmalkar et al., 2020).

Many metropolitan areas across the world experience high traffic congestion, indicating that urban transportation systems are already stressed (Falcocchio and Levinson, 2015). Under these conditions, a relatively small change in traffic flow can trigger spatially extensive disruption because traffic systems are highly non-linear (Kerner, 2012). As demonstrated in prior studies, the closure of even a small percentage of roads, from flooding or otherwise, can propagate congestion throughout the network, leading to region-wide travel time delays (Ganin et al., 2017; Kasmalkar et al., 2020).

Traffic resilience is defined as the ability of the system to withstand traffic disruption, and has been previously estimated in terms of

* Corresponding author.
E-mail address: ineel@alumni.stanford.edu (I. Kasmalkar).

https://doi.org/10.1016/j.uclim.2021.100851
Received 15 February 2021; Received in revised form 1 April 2021; Accepted 13 April 2021
Available online 3 May 2021

travel time delays (Kasmalkar et al., 2020; Ganin et al., 2017). In particular, the study by Kasmalkar et al. Kasmalkar et al. (2020) suggests that areas with dense road networks are more resilient to flood-related travel time delays because they have sufficient alternate road capacity to offset potential increases in traffic volumes. However, solely using the metric of travel time delay for estimating traffic resilience could impart a bias toward travel efficiency rather than road safety into planning efforts. For example, residential communities, especially traditionally disadvantaged communities with limited road-safety measures such as speed bumps, might be more concerned about the risk of accidents on local streets rather than travel time delays.

In this study, we quantify traffic resilience in terms of the change in the rates of non-highway car and pedestrian accidents during the morning commute hours as a result of coastal flooding in the San Francisco Bay Area for the 2020–2040 period. A coastal flood event is defined as an extreme water level that can result from multiple potential combinations of storm surges, tides, seasonal cycles, inter-annual anomalies driven by large-scale climate variability such as the El Niño Southern Oscillation, and near-future sea level rise. Our study is the result of an ongoing stakeholder-engagement process as part of the Stanford Future Bay Initiative and inspired specifically by community members of North Fair Oaks, California, who have highlighted concerns around road safety arising from the large volume of traffic that cuts through their neighborhoods when the nearby highway US-101 is congested. Given these concerns, we choose non-highway car and pedestrian accident rates as proxies for road safety since these two types of accidents pose direct risks to individuals and property within a specific community.

Prior studies show that socioeconomic characteristics have a substantial influence on accident rate (Lee and Abdel-Aty, 2005; Quddus, 2008; Lord and Mannering, 2010; Wang et al., 2013). The San Francisco Bay Area is highly spatially heterogeneous in its socioeconomic characteristics, suggesting that accident rates might be spatially heterogeneous, too. For example, the neighboring cities of Palo Alto and East Palo Alto have markedly different median household incomes, ethnic composition, and educational levels (United States Census Bureau, 2017a). To represent the role of socioeconomic characteristics on accident rates, prior studies use regressions with a variety of socioeconomic variables (Lee and Abdel-Aty, 2005; Quddus, 2008; Lord and Mannering, 2010; Wang et al., 2013), but this approach may overfit data since many socioeconomic variables such as education and income are correlated. Our study, on the other hand, precedes the regression analysis with a clustering approach (Wood et al., 2015; Hummel et al., 2018) to aggregate proximal census blocks with similar median household incomes and free flow travel speeds into contiguous areas, called communities. Clustering reduces the variability in the socioeconomic and road variables within individual communities, allowing us to relate accident rate to the average values of the variables for each community.

Socioeconomic characteristics are not the only variables that affect the accident rates of communities. Traffic volume is important as well, especially in dynamic metropolitan areas where traffic conditions change substantially from hour to hour (Retallack and Ostendorf, 2019). A majority of highway accident studies show either a linearly increasing or a U–shaped profile for the relationship between accident rate and traffic volume (Retallack and Ostendorf, 2019; Gwynn, 1967; Martin, 2002). The relationship has not been studied as extensively for car accidents in urban and suburban settings. One observational study monitoring 120 signal intersections in Adelaide, Australia, found that car accident counts increase with hourly traffic volumes, with an especially sharp increase at very high traffic volumes (Retallack and Ostendorf, 2020). For pedestrian accidents, empirical studies have limited temporal resolution, but existing work suggests that annual accident rates correlate with average annual traffic volumes in an approximately linear way (Lee and Abdel-Aty, 2005; Maycock and Hall, 1984).

Accident rates may depend on multiple factors other than traffic volume and socioeconomic characteristics, including road safety precautions, driver age, and pedestrian volume (Lee and Abdel-Aty, 2005; Retallack and Ostendorf, 2019; Maycock and Hall, 1984; Brüde et al., 1998). However, we assume that over the hourly time scales at which we conduct our analysis of flood-related accident rates and at the spatial scale of communities, the average values of variables other than traffic volume do not vary substantially. Our analysis, therefore, estimates accident rate as a function of traffic volume for each community, and assumes that the underlying relationship is approximately representative of the near-future, defined here as the 2020–2040 period.

Given the relationship between accident rate and traffic volume, our study characterizes the impacts of coastal flooding on accident rate as follows: coastal floodwater inundates low-lying roads and makes them inaccessible, which alters regional traffic volumes by forcing commuters onto alternate roads, subsequently changing accident rates for communities. Flooding also alters accident rates more directly by forcing some commuters to drive in wet road conditions, putting them at risk of hydroplaning (Pregnolato et al., 2017). Extensive wet road conditions are characteristic of pluvial flooding (Pregnolato et al., 2017; Brodsky and Hakkert, 1988). However, unlike pluvial flooding, coastal flooding in the San Francisco Bay Area is projected to inundate a very small proportion of road segments (Kasmalkar et al., 2020), indicating that the exposure to wet road conditions is geographically limited. Our study focuses on coastal flooding rather than pluvial flooding. Thus, our study complements previous studies of accidents caused by wet road conditions (Brodsky and Hakkert, 1988; Qiu and Nixon, 2008; Xu et al., 2013) by estimating the spatially extensive changes in traffic volumes and the subsequent changes in accident rates resulting from coastal flooding, even in areas that experience no direct flooding.

To estimate flood-related accident rates, we use historical accident data over the period 2013–2019 from the Statewide Integrated Traffic Records System (California Highway Patrol, 2019) to derive hourly non-highway car and pedestrian accident rates for each community for the five time periods 5–6 am, 6–7 am, 7–8 am, 8–9 am, and 9–10 am. We then simulate morning traffic patterns in the San Francisco Bay Area, both in the presence and absence of coastal flooding, using an incremental traffic assignment model (Kasmalkar et al., 2020). We derive regressions from the hourly trends in modeled traffic volumes and historical accident rates over the weekday 5–10 am time period, and use the regressions to estimate accidents rates in the presence of flooding.

The estimated accident rates represent one possible quantification of the resilience of communities in the San Francisco Bay Area to the impacts of near-future coastal flooding on the traffic system. While traffic resilience has been previously quantified in terms of travel time delays (Kasmalkar et al., 2020; Ganin et al., 2017; Suarez et al., 2005), our study highlights the complex, multi-faceted nature of traffic resilience and emphasizes the need for incorporating road safety into climate adaptation planning.

2. Model

2.1. Dividing the region into communities

Census blocks provide an initial basis for partitioning the San Francisco Bay Area (United States Census Bureau, 2018). However, many census blocks have zero reported accidents for the 5–10 am time period studied here because of their relatively small sizes. We use k-means clustering to aggregate geographically proximal census blocks with similar median household incomes and mean free flow travel speeds into larger contiguous areas, called communities. Free flow travel refers to the condition of a car traveling on a road segment in the absence of congestion or other adverse driving conditions. We estimate free flow travel speeds over road segments from

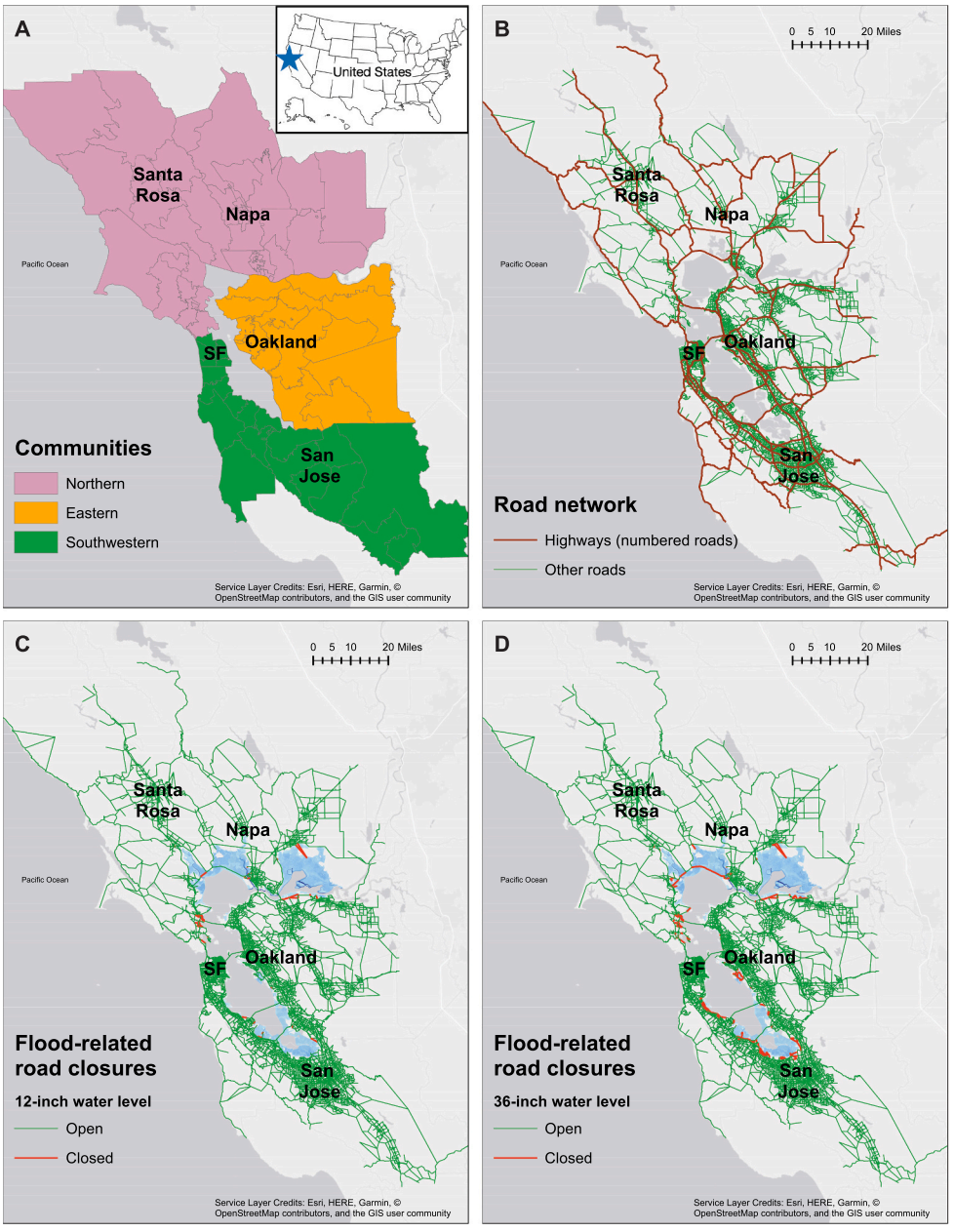

Fig. 1. The San Francisco Bay Area, USA. (A) The San Francisco Bay Area, divided into 72 communities. The cities of Napa, Oakland, San Francisco (labeled SF), San Jose, and Santa Rosa are shown for reference. (B) The regional road network with highways shown in brown. We consider any numbered road to be a highway. (C, D) The flood map and projected road closures for the 12– and 36–inch water levels, respectively. (For interpretation of the references to colour in this figure legend, the reader is referred to the web version of this article.)

the San Francisco Bay Area Metropolitan Transportation Commission's regional road network (Metropolitan Transportation Commission/Association of Bay Area Governments (MTC/ABAG), 2017) and average them at the scale of census blocks. We obtain the median household income values for census blocks from the American Community Survey (United States Census Bureau, 2017a). By clustering census blocks, we partition the San Francisco Bay Area into a total of 72 communities, shown in Fig. 1. The spatial extents of communities are large enough to have non-zero car and pedestrian accident counts, yet small enough to reflect the spatial heterogeneity in socioeconomic and road characteristics of the region.

2.2. Simulating traffic patterns with flooding

We use the traffic model developed by Kasmalkar et al. Kasmalkar et al. (2020) to simulate traffic patterns in the San Francisco Bay Area. The traffic model simulates traffic volumes at the scale of individual road segments, which are subsequently aggregated to the community level. The traffic model uses two inputs, namely, the San Francisco Bay Area Metropolitan Transportation Commission's road network, shown in Fig. 1B (Erhardt et al., 2012), and the Longitudinal Employer–Household Dynamics Origin–Destination Employment Statistics (LODES) dataset (United States Census Bureau, 2017b) which provides home–work location pairs for commuters at the census block level. To assign commuters to their home-to-work routes, the model uses an incremental traffic assignment algorithm which partitions the set of commuters in the LODES dataset uniformly and proportionally into batches of size 40%, 30%, 20%, and 10%, and sequentially assigns the commuters to their shortest routes one batch at a time (Chen and Alfa, 1991; Wang et al., 2012).

The traffic model uses an empirical function which estimates how travel time changes with traffic volumes for individual road segments (United States Bureau of Public Roads, 1964; Branston, 1976),

$$t = t_0(1 + \alpha(V/C)^{\beta}), \tag{1}$$

where t is the travel time for a given road segment, t_0 is the free flow travel time for the road segment, V and C are the traffic volume and capacity of the road segment, measured in cars/hr, and α and β are parameters. In this study, we set these parameters to $\alpha = 0.2$ and $\beta = 6.0$, as suggested by the Metropolitan Transportation Commission (Erhardt et al., 2012). We impose 80 miles/hr and 5 miles/hr as the respective upper and lower bounds on the travel speeds for each road segment. We only consider private cars and do not account for public transit (Kasmalkar et al., 2020). We also neglect traffic signals, stop signs, tolls, and carpool lanes, and do not account for travel time delays resulting from accidents.

The traffic model by Kasmalkar et al. (Kasmalkar et al., 2020) simulates traffic patterns over the time period of a single hour, but our analysis of accident rates requires traffic simulations that span the entire morning commute period of 5–10 am. Traffic flow over multiple hours may exhibit the potential temporal spillover of traffic, where, for example, traffic congestion during the 8–9 am time period may impact the traffic patterns over the 9–10 am time period. To capture the temporal spillover of traffic, we modify the model so that commuters whose travel times exceed one hour are retained in the simulation over the successive hour. For example, if 1000 commuters traveling on a particular road segment in the 7–8 am time period have travel times that exceed one hour, then the simulation for the 8–9 am time period is initiated with a traffic volume of 1000 on that road segment. We estimate the number of commuters initiating their commutes in each hour of the 5–10 am time period from the American Community Survey (see Table A.1).

To identify roads within the traffic system that may be closed as a result of coastal flooding, we use the method of Kasmalkar et al. Kasmalkar et al. (2020) where we overlay coastal flood maps on the road network, correct for potential biases in road geometry, elevation, and representations of road-creek crossings, and close down road segments with more than 3 in. of water at any point along their extents. Similar to (Kasmalkar et al., 2020), we use the San Francisco Bay Department of Conservation and Development Commission's Adapting to Rising Tides (ART) flood maps, which represent extreme water levels resulting from multiple potential combinations of storm surges, tides, seasonal cycles, inter-annual anomalies driven by large-scale climate variability such as the El Niño Southern Oscillation, and near-future sea level rise (Vandever et al., 2017). For example, the 36–inch water level flood map can represent both a 50-yr return period coastal flood at present-day sea level, as well as a 20-yr coastal flood on top of 6 in. of sea level rise (Kasmalkar et al., 2020; Vandever et al., 2017). Our study considers the ART flood maps corresponding to the 12–, 24–, and 36–inch water levels. The 12– and 36–inch flood maps are shown in Figs. 1C and D, respectively.

2.3. Deriving the statistical relationship between traffic volume and accident rate

We choose the weekday 5–10 am time period for the analysis of the relationship between traffic volumes and accident rates of communities. The 5–10 am window represents a period of substantial and relatively predictable traffic activity. During the 5–10 am time period, over 90% of the regional workforce travels between fixed origins and destinations, namely, home and work (United States Census Bureau, 2017a). Approximately 20% of the non-highway car and pedestrian accidents occur during the 5–10 am time period, indicating the importance of this time period in the context of community road safety (California Highway Patrol, 2019).

The Statewide Integrated Traffic Records System is a standardized platform used by the California Highway Patrol and its allied agencies for collecting and storing geolocated car and pedestrian collision reports across the State of California (California Highway Patrol, 2019). From the records system, we select non-highway car and pedestrian accidents within the 9 counties of the San Francisco Bay Area and during the weekday 5–10 am period over January 2013–December 2019. Highways are defined as roads with officially designated numbers (see Fig. 1B). We map the accident locations to the respective communities in which they occur, sum over the number of accidents, and divide by the total number of working days over the 2013–2019 period to get the historical hourly non-

highway car and pedestrian accident rates for each community for each of the five hours. We only consider communities with accident data in at least four out of the five individual hours in the 5–10 am period to ensure at least four data points for our regression analysis. Therefore, we remove communities where accident data is unavailable for more than one out of the five hours from our analysis. Of the 72 communities designated in our study, 64 communities have sufficient data for our analysis of non-highway car accidents and 45 communities have sufficient data for our analysis of pedestrian accidents.

We compute the average non-highway traffic volume of a community by averaging the traffic volumes of all the non-numbered road segments intersecting the geographical extent of the community while weighting each road segment by its length. Since our analysis does not include accidents caused directly by wet road conditions, we only include non-flooded road segments when computing average traffic volumes. For each community, and for both non-highway car and pedestrian accidents, we use linear and quadratic regressions to fit curves through the points determined by average non-highway traffic volumes and the hourly non-highway accident rates without flooding for each of the five hours in the 5–10 am period. The choice of linear and quadratic regressions is motivated by their relative simplicity, as well as prior empirical studies that find these two relationships most commonly between accident rates and traffic volumes (Retallack and Ostendorf, 2019). Between the linear and quadratic regression curves, we select the one with the higher adjusted R^2 coefficient. We then use the selected regression curve for each community to estimate the likely accident rate based on the traffic volumes projected for the 12–, 24–, and 36–inch water levels.

Since our model does not analyze highway accidents, we use the term "accidents" to refer to non-highway accidents from this point onward. Similarly, we use the term "traffic volumes" to refer to traffic volumes on non-highway roads only.

3. Validation of modeled travel times

In our regression analysis, we relate historical accident rates to modeled traffic volumes. The validity of this approach hinges on the accuracy of the model and raises the question of potential biases that could be introduced by the model being more accurate in some time periods than in others. We compare modeled travel times in the absence of flooding against historical travel times provided by the TomTom routing system (TomTom, 2020). The TomTom routing system uses historical Global Positioning System–based travel data to estimate the average travel time for a given origin-destination pair at a given time of departure (TomTom, 2020). In Figs. 2A and B, we plot histograms of the differences in travel times computed by our traffic model and those estimated by TomTom over all road segments in our road network. We present the results for the 6–7 am time period, which is representative of the non-peak hour traffic (5–7 am), and the 8–9 am time period, which is representative of peak hour traffic (7–10 am). The histograms for both the 6–7 am and 8–9 am time periods have means less than 2.5 min and standard deviations less than 3.5 min. The histograms show skewed distributions, indicating larger travel times for TomTom than for our traffic model. The histograms for the other three hours show similar results (see Fig. C.1).

While Figs. 2A and B compare TomTom and modeled travel times at the scale of individual road segments, the focus of our study lies at the scale of communities. To identify potential systematic biases in travel times at the community scale, we plot the histograms of the differences in TomTom and modeled travel times averaged across communities in Figs. 2C and D. We compute the average travel time for a given community by summing the travel times of all the road segments intersecting the community and dividing by the sum of the lengths of the road segments. The normalization by road segment length provides a meaningful comparison across communities of different sizes. The panels C and D show single-peak distributions of average travel times for the 6–7 am and 8–9 am time periods,

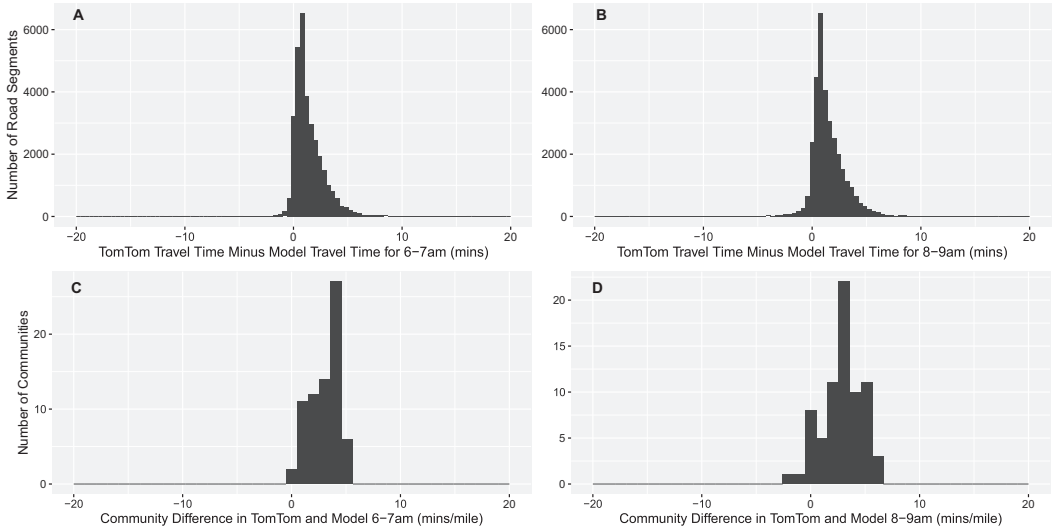

Fig. 2. Comparing modeled travel times against TomTom estimates. (A, B) Histograms over all segments in the model road network for differences in TomTom and modeled travel times for 6–7 am and 8–9 am, respectively. (C, D) Histograms over all 72 communities for differences in average TomTom and modeled travel times for 6–7 am and 8–9 am, respectively.

respectively, where the latter has a more pronounced peak. Both the distributions have averages of approximately 3.2 min per mile, and standard distributions of approximately 1.4 min per mile.

All the histograms in Fig. 2 show larger travel times for TomTom than for our model, a consequence of the optimal travel conditions assumed in our model. Our road network contains simplified road segments that do not correspond to real roads (Erhardt et al., 2012), thus providing slightly shorter routes for commutes. Our model also does not consider travel time delays caused by adverse road conditions such as constructions sites or accident locations.

To demonstrate that the difference between TomTom and modeled travel times has a small, uniform, and systematic bias, we subtract 3 min per mile for each road segment from the TomTom travel times and plot the altered histograms in Fig. 3. The histograms show approximately symmetric distributions centered at 0, indicating a reduction of the bias. We do not make any adjustments for the bias when performing the regression analyses in this study.

4. Aleatoric uncertainty in modeled traffic volumes

Incremental traffic models compute traffic volumes by optimizing travel times across the road network (United States Bureau of Public Roads, 1964; Branston, 1976). Our model relates travel time to traffic volume using power-law functions involving two parameters, α and β, as seen in Eq. (1). There is, however, considerable uncertainty in the parameters. Our model follows the choices of the San Francisco Bay Area Metropolitan Transportation Commission, $\alpha = 0.2$ and $\beta = 6.0$ (Erhardt et al., 2012). Prior studies of hazard-related traffic disruption have used different values, e.g., $\alpha = 0.15$ and $\beta = 4.0$ (Miller and Baker, 2016; Kasmalkar et al., 2020). Some studies report a range of values, with $0.1 < \alpha < 0.4$ and $4.0 < \beta < 6.0$ (Branston, 1976; Kim and Mahmassani, 1987), while others present even wider ranges (Mtoi and Moses, 2014).

To estimate the aleatoric uncertainty in modeled traffic volumes, we conduct 20 traffic simulations, with $\alpha = 0.15,0.3,0.5,0.7$ and $\beta = 4.0,4.5,5.0,5.5,6.0$. For each of the 72 communities, we compute the relative standard deviation of the average traffic volumes computed for the range of values of α and β for a given hour. We plot the results in Fig. 4, where each point represents the relative standard deviation of traffic volume for a given community over a given hour. The figure shows that the relative standard deviation values of the communities range from 0 to 80%. For each community, the relative standard deviation is the smallest for the 5–6 am time period, when congestion is relatively low and most cars travel under free flow conditions. On the other hand, the relative standard deviation is largest for the 9–10 am time period for almost all communities. Most of the traffic in the 9–10 am time period consists of the congested traffic that initiated its commute in the prior time periods (see Table 1). Our results suggest that the modeled volumes of the congested traffic from prior time periods are highly sensitive to the choice of parameters, resulting in large standard deviation values during the 9–10 am time period.

We account for the aleatoric uncertainty in traffic volumes by using the relative standard deviation values to construct 95% confidence intervals around the modeled traffic volumes ($\alpha = 0.2$, $\beta = 6.0$) for each community.

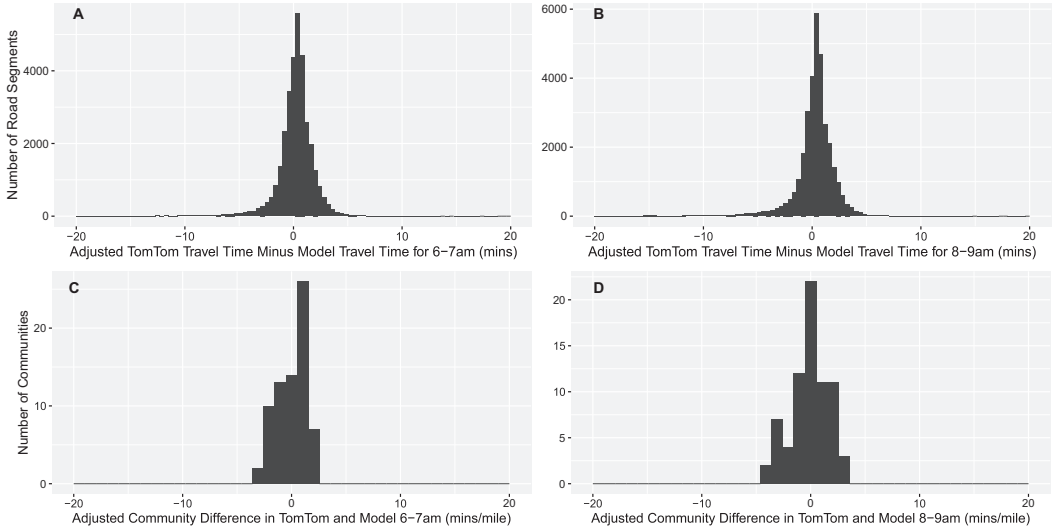

Fig. 3. Adjusted histograms for the differences in TomTom and modeled travel times. The differences are adjusted by 3 mins/mile. (A, B) Histograms over all segments in the model road network for differences in TomTom and modeled travel times for 6–7 am and 8–9 am, respectively. (C, D) Histograms over all 72 communities for differences in average TomTom and modeled travel times for 6–7 am and 8–9 am, respectively.

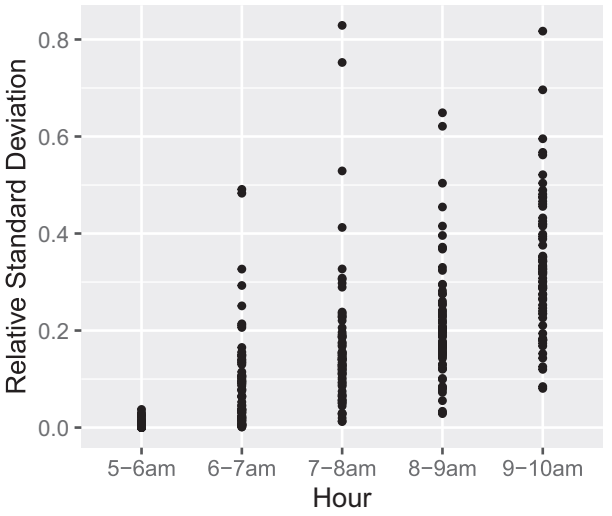

Fig. 4. The relative standard deviation of traffic volumes for communities over each time period. Each point corresponds to a community for a given hour.

5. Results

5.1. Accident rates increase with traffic volumes for most communities

To constrain the relationship between accident rates and traffic volumes, we compute the corresponding linear and quadratic regression curves for each community. We estimate the average traffic volumes from the model described in Section 2 and obtain the accident rates from the accident records system (California Highway Patrol, 2019). We show the regression curves of four example communities in Fig. 5. We compute the vertical errors bands representing the 95% confidence intervals from the standard errors of the underlying least squares regressions. We compute the horizontal error bars representing the 95% confidence intervals from the relative

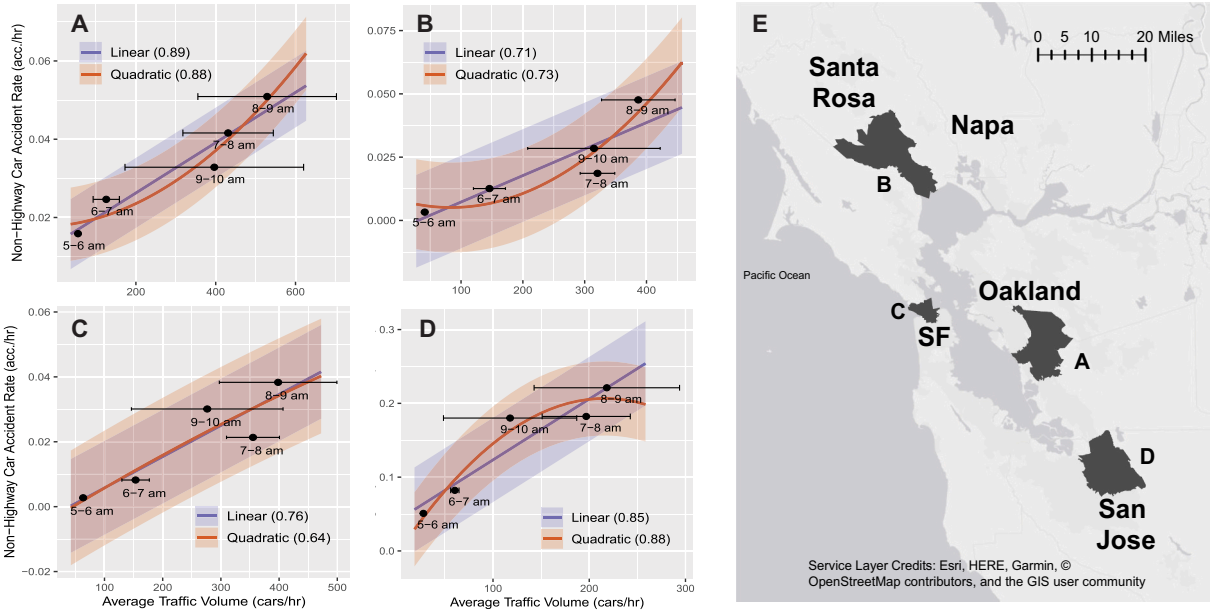

Fig. 5. Regression curves of traffic volumes and non-highway car accident rates for 4 communities, shown in panels A, B, C, and D. Black dots indicate historical car accident rates with modeled traffic volumes. The blue curves represent the best-fitting linear regressions and the orange curves represent the best-fitting quadratic regressions. The adjusted R^2 coefficients for the respective regressions are shown in parentheses in the legend. (E) Locations of the four communities. (For interpretation of the references to colour in this figure legend, the reader is referred to the web version of this article.)

standard deviations of the modeled traffic volumes (Fig. 4). The largest traffic volumes correspond to the 8–9 am time period (Table A.1). The largest confidence intervals for traffic volumes correspond to the 9–10 am time period, a consequence of the high uncertainty in modeled traffic volumes for the relatively large temporal spillover of traffic from prior time periods (Fig. 4).

For each community, we choose either the linear or the quadratic regression based on the higher adjusted R^2 coefficient. Panel A of Fig. 5 shows a community near the city of Hayward, California with five data points of car accident rates and traffic volumes. We choose the linear regression because it has a higher adjusted R^2 coefficient (adj. $R^2 = 0.89$) than for the quadratic regression (adj. $R^2 = 0.88$). In panel B, which shows a community near the city of Santa Rosa, the quadratic regression is chosen instead. Panel C, representing a community in San Francisco City, shows near-identical linear and quadratic regression curves. The latter has a lower adjusted R^2 coefficient since it provides a similar fit despite using a higher degree polynomial. In panel D, which shows a community in the city of San Jose, the linear regression has an increasing trend while the quadratic regression has the shape of an inverted U, where we select the latter for its higher adjusted R^2 coefficient.

Fig. 6A summarizes our model choices of regression curves for all communities in the San Francisco Bay Area. Among the 64 communities with sufficient car accident data, 40 have increasing linear profiles, 10 have U-shaped quadratic profiles and 14 have inverted U-shaped profiles. Although linear and U-shaped profiles are found most commonly in prior studies (Retallack and Ostendorf, 2019; Martin, 2002), there is some evidence for inverted U-shaped profiles in prior studies (Veh, 1937; Raff, 1953). Overall, our results suggest that most communities have an increasing relationship between car accident rates and traffic volumes.

The fit between the chosen regression curves and the relationship between observed car accident rates and modeled traffic volumes also vary spatially, as demonstrated by the R^2 coefficients for each community in Fig. 6B. Of the 64 communities with sufficient car accident data, 34 have R^2 coefficients of 0.9 or higher, and 3 have coefficients lower than 0.5. We discard the 3 communities with R^2 coefficients lower than 0.5 from our car accident analysis, because we are unable to identify a relationship between car accident rates and traffic volumes for these.

The spatial distributions of the profiles and the R^2 coefficients depend on the clustering used to partition the region into communities. To understand the degree to which clustering affects the distributions in Fig. 6, we present results for two alternate clusters in the Appendix, Fig. D.1. The two alternate clusters represent opposing end members of clustering, where one prioritizes the proximity of census blocks, while the other prioritizes similar median household incomes and free flow travel speeds over proximity. Comparing Fig. 6 and Fig. D.1, we note that most communities have linearly increasing relationships between accident rates and traffic volumes for both the original and alternate clustering approaches. For the majority of communities, the different clustering approaches suggest similar profiles, but there are prominent exceptions. For example, communities around San Francisco City have a mix of linearly increasing and inverted U-shaped profiles which change with the specific clustering approach. The choice of the clustering approach affects the profiles assigned to communities on the cusp of different behaviors, such as a switching a linear profile to either a mildly U-

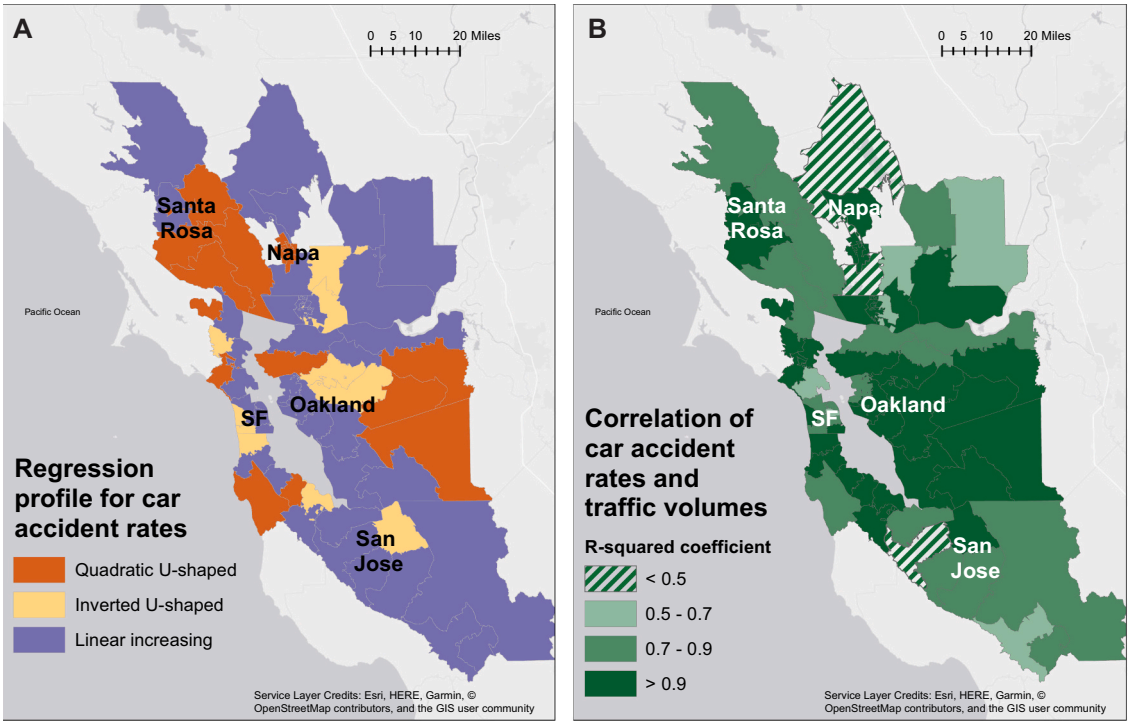

Fig. 6. Spatial distribution of the regression curves for non-highway car accident rates and traffic volumes. (A) Profile of the quadratic regression, either U-shaped, inverted U-shaped, or linearly increasing. (B) The R^2 coefficients. We remove the 3 striped communities from the analysis because of their low R^2 coefficients.

shaped or inverted U-shaped profile. The spatial distributions of the R^2 coefficients are also approximately similar at the regional scale for the various clustering approaches. Overall, our analysis suggests that the choice of the clustering approach may alter our results at the community scale, particularly in places like San Francisco City, but has limited impact on our results at larger spatial scales.

We perform a similar analysis for pedestrian accident rates. In Fig. 7, we show the regression curves between pedestrian accident rates and traffic volumes for the four communities shown in Fig. 5E. Similar to the case for car accident rates, the linear regression curves for pedestrian accidents are increasing in all four panels. We choose a regression model based on the same rationale of higher adjusted R^2 coefficients as for car accidents. We find that the selected regression profiles for the car accident rates, linear versus quadratic, do not necessarily resemble the regression profiles for the pedestrian accident rates. Our results suggest that the dynamics for car accidents are notably different from those of pedestrian accidents in the San Francisco Bay Area.

We present the distributions of the profiles and R^2 coefficients of the regression curves for the pedestrian accident rates in Fig. 8. Out of the 45 communities which have sufficient pedestrian accident data, 24 have a linearly increasing profile, 10 have a quadratic U-shaped profile, and 11 have an inverted U-shaped profile (panel A). There are 16 communities with R^2 coefficients greater than 0.9. There are 7 communities with R^2 coefficients lower than 0.5, which we remove from our pedestrian accident analysis.

The Figs. 6 and 8 show that most communities have increasing relationships between accident rates and traffic volumes, which is consistent with prior studies (Retallack and Ostendorf, 2019). The figures also show that there is considerable variability between the regression curves across the various communities. The underlying heterogeneity of the region contributes to the variability in the regression curves between accident rates and traffic volumes. Communities may differ substantially in socioeconomic conditions, driving norms, traffic infrastructure, and accident reporting, all of which influence car and pedestrian accident rates (Lee and Abdel-Aty, 2005; Lord and Mannering, 2010; Retallack and Ostendorf, 2019).

5.2. *Coastal flooding exacerbates peak-hour accident rates*

Coastal flood events have the potential to prompt the closure of low-lying roads in the San Francisco Bay Area, subsequently disrupting regional traffic patterns (Kasmalkar et al., 2020). To estimate changes in accident rates as a consequence of flood-related changes in traffic volumes, we use the regression curves from Section 5.1 with modeled traffic volumes in the presence of flooding.

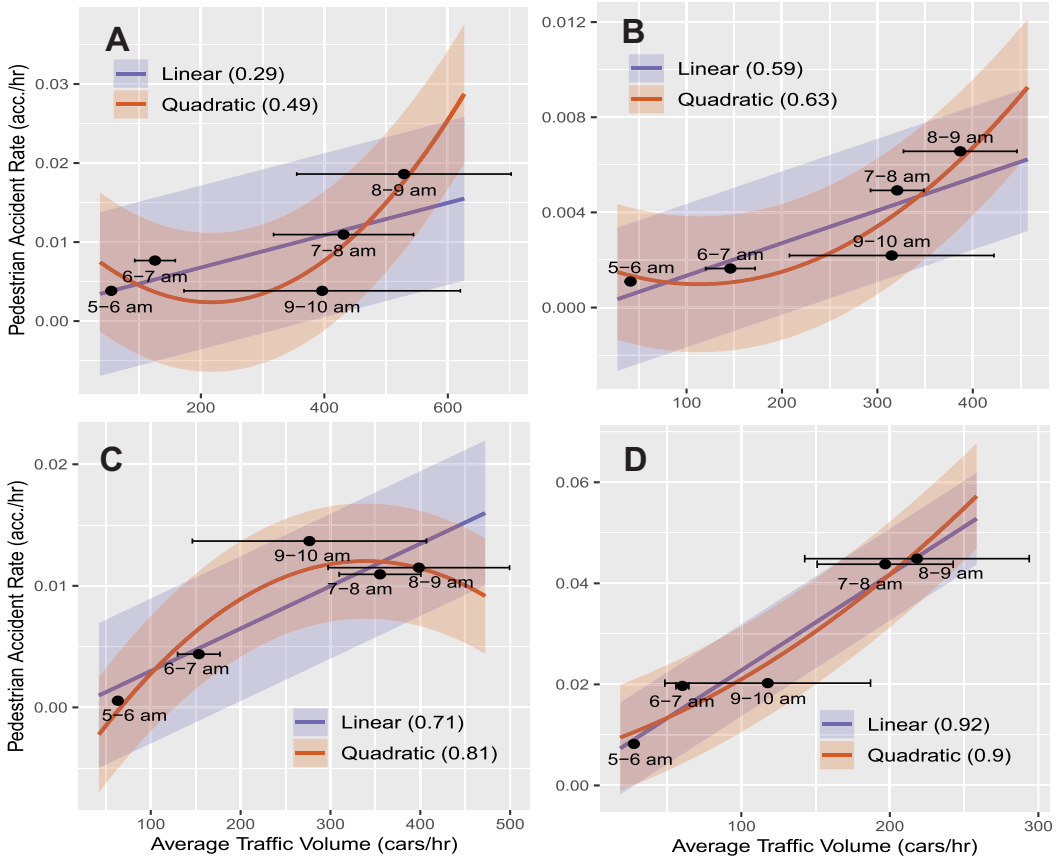

Fig. 7. Regression curves of traffic volumes and pedestrian accident rates for the 4 communities shown in Fig. 5E. The adjusted R^2 coefficients for the respective regressions are shown in parentheses in the legend.

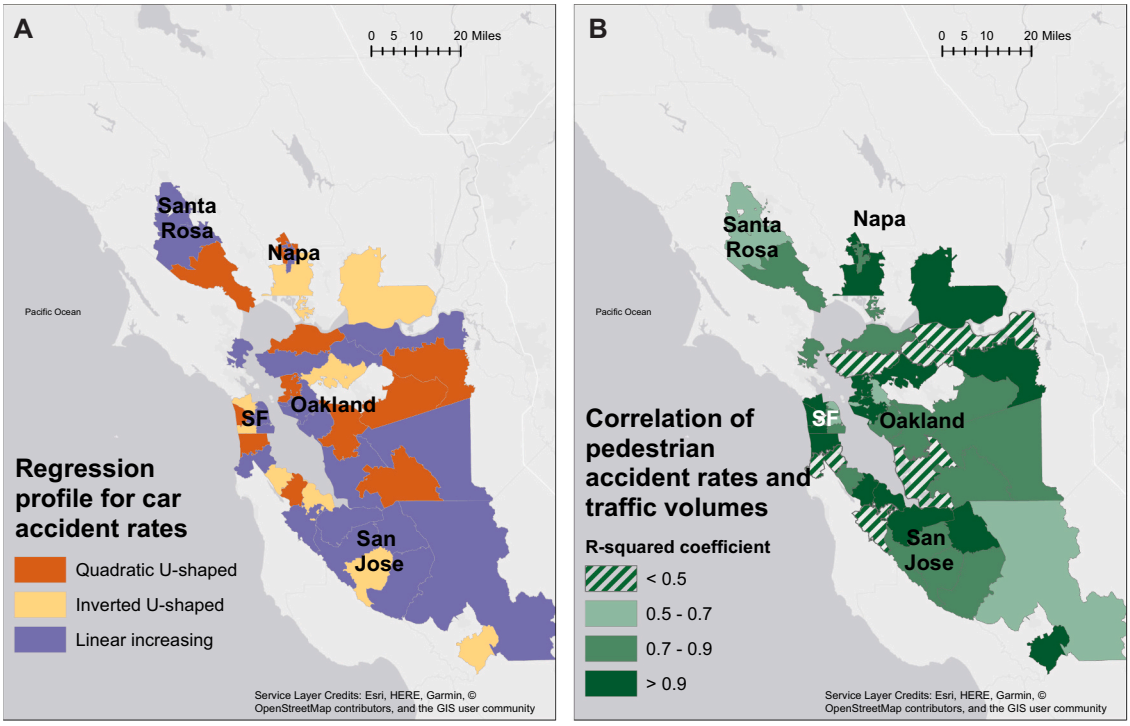

Fig. 8. Spatial distribution of the regression curves for pedestrian accident rates and traffic volumes. (A) Profile of the quadratic regression, either U-shaped, inverted U-shaped, or linearly increasing. (B) The R^2 coefficients. We remove the 7 striped communities from the analysis because of their low R^2 coefficients.

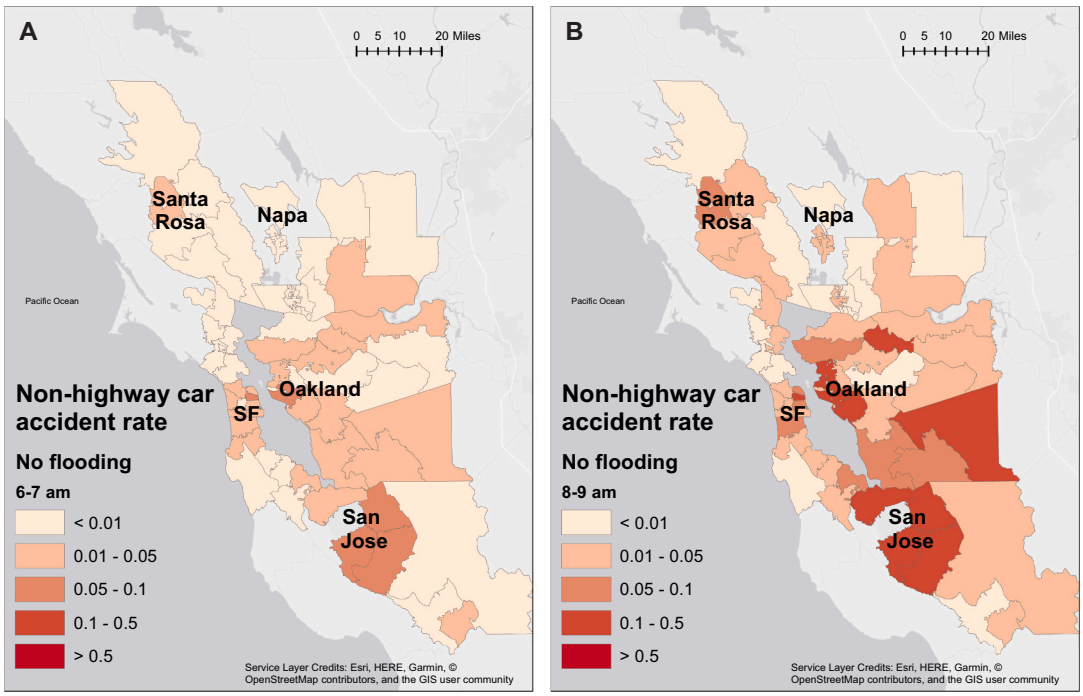

Fig. 9. Computed non-highway car accident rates without flooding, by community. (A) 6–7 am time period. (B) 8–9 am time period. Of the 72 communities, 8 are removed for lack of accident data, and 3 are removed for having R^2 regression coefficients less than 0.5.

To establish baseline accident rates, we first compute the car accidents rates without flooding for each community and plot the results for the 6–7 am and 8–9 am time periods in Fig. 9. An accident rate of 0.05 accidents/hr in the 6–7 am time period means that there is one accident approximately every 20 days in the 6–7 am time period. Panels A and B are representative of the spatial distribution of non-peak hour (5–7 am) and peak hour (7–10 am) accident rates, respectively. During the 6–7 am time period, most of the communities with relatively high car accident rates are located in the southern Bay (0.05–0.1 accidents/hr). With the exception of one community near the city of Santa Rosa, the northern communities have relatively low accident rates (<0.01 accidents/hr). Most

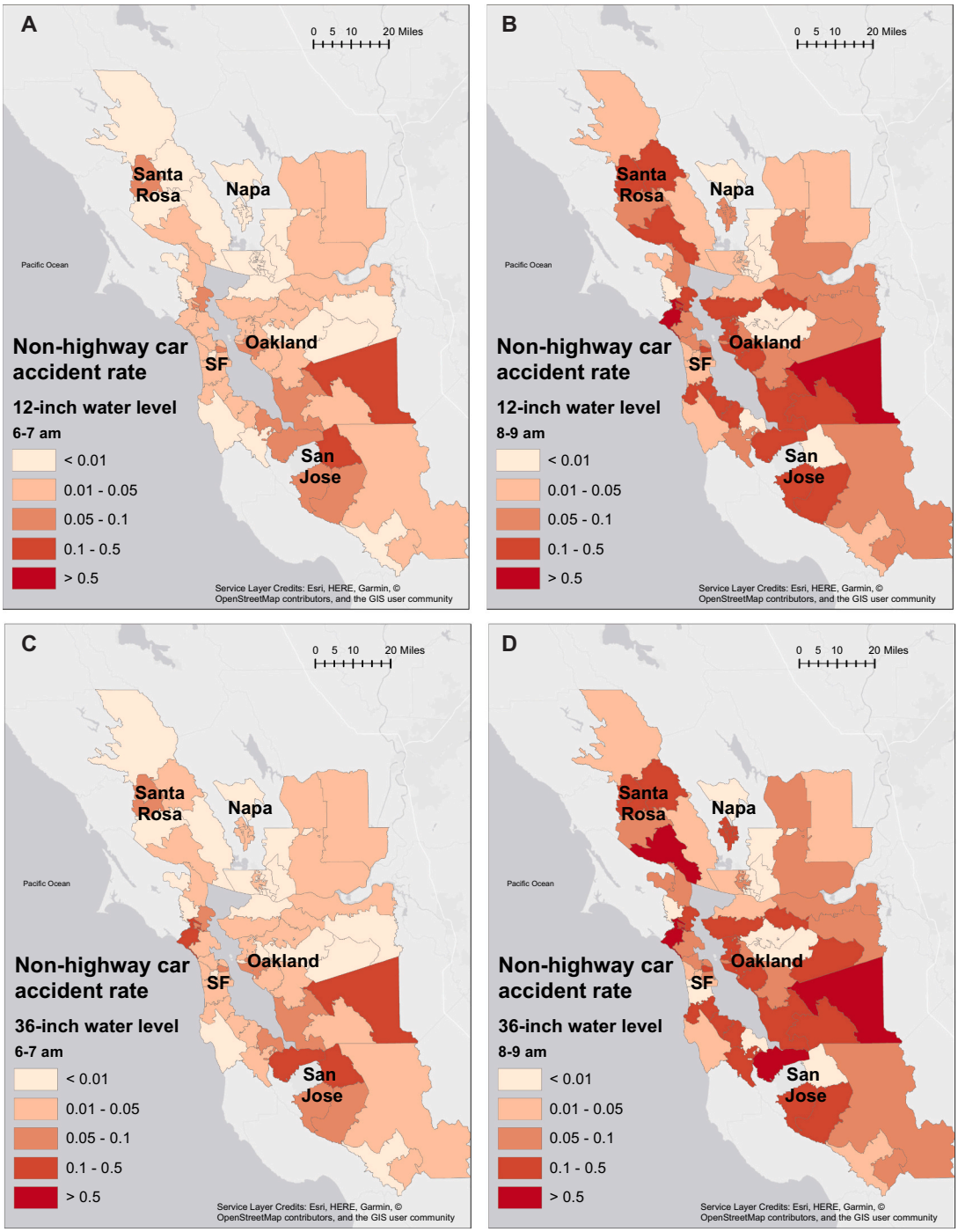

Fig. 10. Model estimates of the non-highway car accident rates with flooding, by community. (A, B) 6–7 am and 8–9 am, respectively, for the 12–inch water level. (C, D) Same as (A, B), for the 36–inch water level.

communities have higher car accident rates in the 8–9 am time period than in the 6–7 am time period (Fig. 9). Communities in the eastern and southwestern region (Fig. 1A), especially those around the cities of Oakland and San Jose, have the highest increases in accident rates during peak hours.

To estimate how accident rates change with flooding, we assume that flooded roads are closed to traffic (Fig. 1), simulate traffic patterns, and use the regression curves to estimate accident rates for communities. Our results in Fig. 10 show that, for most communities, car accident rates with flooding are higher than those without flooding (Fig. 9). Relative to the baseline, the 6–7 am car accident rates increase the most for southwestern and eastern communities, especially those around the cities of Oakland and San Jose. The 6–7 am accident rates are approximately similar for the two water levels, 12 and 36 in. (Fig. 10A and C).

For the 8–9 am time period, the car accident rates for both the 12– (Fig. 10B) and 36–inch water levels (Fig. 10D) increase substantially as compared to the 6–7 am time period. The increases are higher for the 36–inch water level, especially in communities around the cities of Napa, San Jose, and Santa Rosa. The increase in car accident rates from 6–7 am to 8–9 am is substantially greater in the presence of flooding (Fig. 10) than in the absence (Fig. 9), suggesting that flooding exacerbates peak-hour accident rates.

We conduct a similar analysis for pedestrian accident rates. In Fig. 11, we plot the pedestrian accident rates without flooding. The pedestrian accident rates are very low (<0.01 accidents/hr) for most communities. Most of the pedestrian accidents are concentrated in the communities around the cities of Oakland, San Francisco, and San Jose. We show the pedestrian accident rates with flooding in Fig. 12. Relative to the baseline rates, the 6–7 am rates increase slightly with flooding, where the increases occur in the communities around the cities of Oakland, San Francisco, and San Jose. Similar to the case of car accidents, the 8–9 am pedestrian accident rates are substantially higher than the 6–7 am accident rates during flooding (Fig. 12) as compared to the baseline (Fig. 11). Most of the 8–9 am pedestrian accidents are concentrated around the cities of Santa Rosa, Napa, Oakland, San Jose, and San Francisco.

The potential errors in historical accident data and modeled traffic volumes (Figs. 5 and 7) create corresponding uncertainty in the regressions used to estimate accident rates. To demonstrate that our results are robust to the uncertainty in the regression, we present car and pedestrian accident rates using only linear regressions in Fig. E.1 and E.2, respectively. The results show very similar distributions of accident rates to Figs. 10 and Figs. 12. The largest differences in accident rates are seen for communities with inverted U-shaped regression profiles, but these communities are limited in number. Overall, our results suggest that small variations in the regressions do not notably alter our model estimates of accident rates.

5.3. *The region-wide accident rates increase substantially at low water levels*

While the previous Section 5.2 presents accident rates at the scale of individual communities, the current Section aggregates the accident rates at a regional scale. We compute the region-wide car and pedestrian accident rates for various water levels and for each of the five time periods by summing over the accident rates of all communities, and present the results in Fig. 13.

The region-wide car accident rate without flooding is smallest for the 5–6 am time period (0.5 accidents/hr). The accident rate then

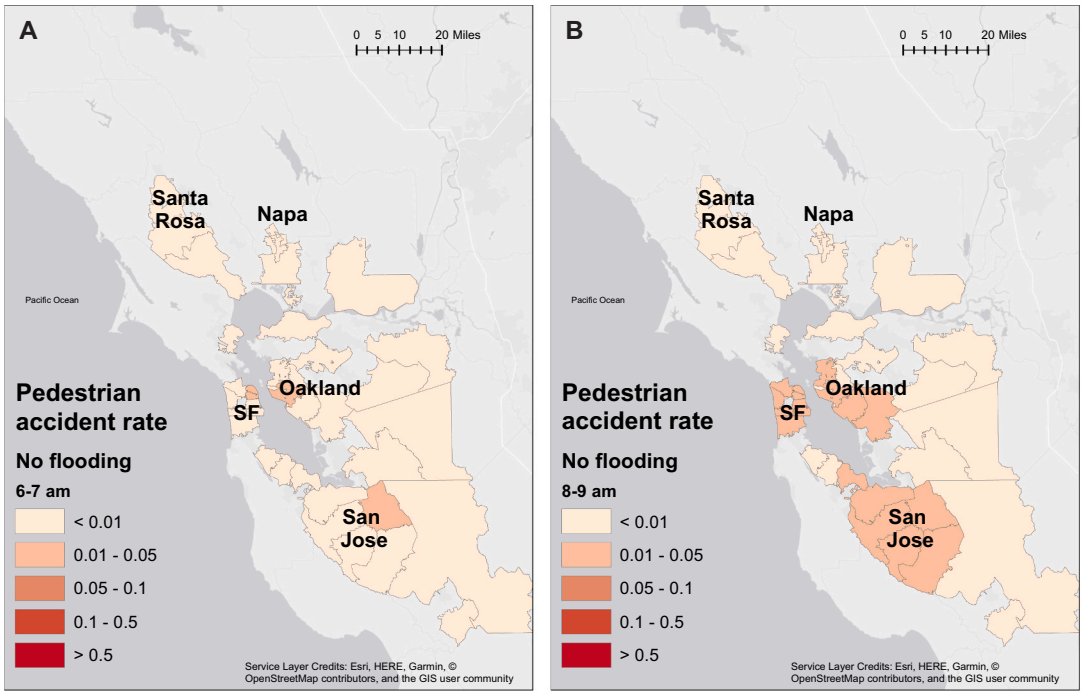

Fig. 11. Computed pedestrian accident rates without flooding, by community. (A) 6–7 am time period. (B) 8–9 am time period. Of the 72 communities, 27 are removed for lack of accident data, and 7 are removed for having R^2 coefficients less than 0.5.

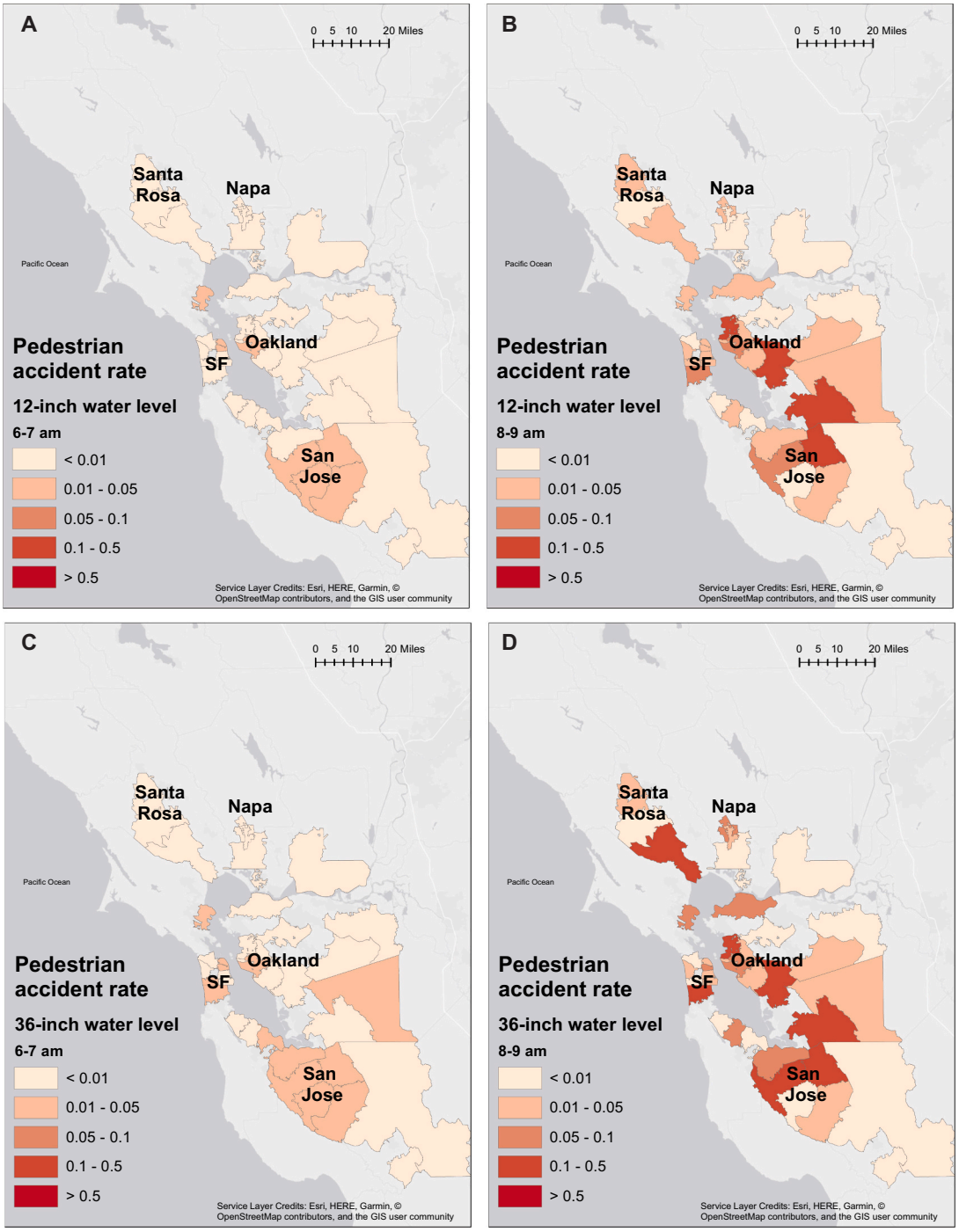

Fig. 12. Model estimates of pedestrian accident rates with flooding, by community. (A, B) 6–7 am and 8–9 am, respectively, for the 12–inch water level. (C, D) Same as (A, B), for the 36–inch water level.

increases gradually until the 8–9 am time period (3.0 accidents/hr), after which it dips slightly for the 9–10 am time period (2.0 accidents/hr). The accident rate for the 12–inch water level follows a similar pattern as that without flooding for the different time periods, but the magnitudes of the accident rates are higher. The accident rate is smallest for the 5–6 am time period (0.9 accidents/hr), increasing up to 7.5 accidents/hr for the 8–9 am time period, and dipping back to 6.0 accidents/hr for the 9–10 am time period. While the magnitude of the accident rate increases with the water level rising to 24 and 36 in., the increase in the accident rate decreases with each successive water level, suggesting that the biggest increase in the region-wide car accident rate occurs at the 12–inch water level,

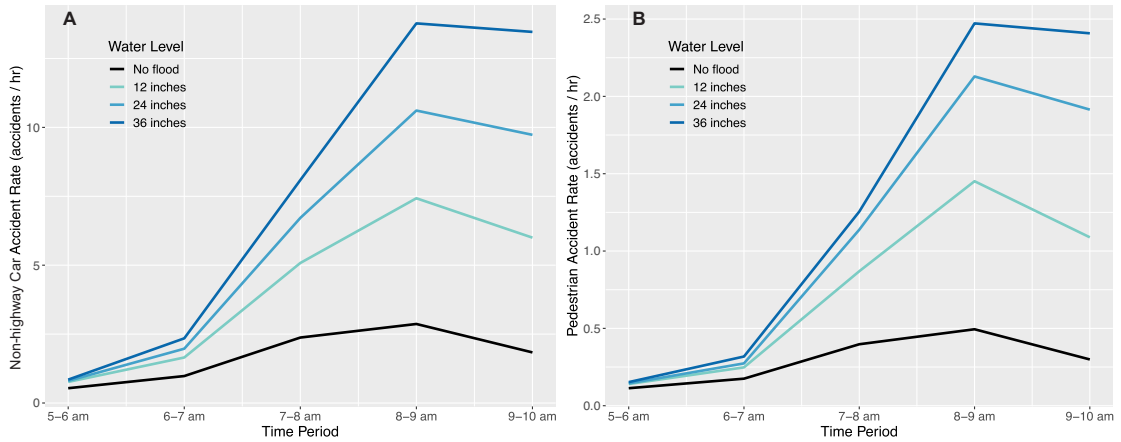

Fig. 13. Cumulative accident rates for the region, estimated for various water levels and hourly time periods. (a) Non-highway car accidents rates. (b) Pedestrian accident rates.

especially during peak hours (7–10 am).

The region-wide pedestrian accident rates, shown in Fig. 13B, exhibit similar trends as the non-highway car accidents rates. The magnitudes of the pedestrian accident rates are substantially lower than those of the non-highway car accident rates because of lower baseline numbers. The total number of recorded pedestrian accidents in the San Francisco Bay Area during the weekday 5–10 am time period are approximately one-fifth of the non-highway car accidents (see Table B.1).

To validate our finding that non-highway car and pedestrian accident rates increase with water level, we present a preliminary analysis in Appendix F where we compute the historical accident counts on flood days, namely, the days where the water levels are greater than 12 in. during the peak hour 7–10 am time period. The historical data has limitations, for example, there are only 7 days in the 2013–2019 period with high water levels, and none of those days have water levels exceeding 18 in.. Nevertheless, our results show that non-highway car accident counts are slightly higher on flood days than across all days. The results for the pedestrian accident counts are less conclusive.

6. Discussion

The urban traffic system, which is central to the functioning of metropolitan regions, is at risk of disruption from a rising sea level and intensifying coastal floods (Kasmalkar et al., 2020; Suarez et al., 2005; Koetse and Rietveld, 2009). The traffic system is interconnected and non-linear, with disruptions propagating rapidly and extensively throughout the network (Kasmalkar et al., 2020; Kerner, 2012; Ganin et al., 2017; Pescaroli and Alexander, 2016). To quantify the ability of a traffic system to withstand disruption, prior studies (Ganin et al., 2017; Freckleton et al., 2012) have developed the concept of traffic resilience. Quantifying traffic resilience, however, remains a challenge given the complex nature of traffic systems.

Previous studies have quantified traffic resilience in terms of travel time delay (Kasmalkar et al., 2020; Ganin et al., 2017). These studies simulate regional traffic patterns and estimate the changes in travel time for commuters resulting from road closures (Kasmalkar et al., 2020; Ganin et al., 2017). Using the metric of travel time delay, however, provides only a partial picture of resilience, one that is focused on travel efficiency. Our study presents an alternate picture of traffic resilience, one that is focused on road safety. We quantify changes in road safety for communities in the San Francisco Bay Area by estimating the rates of non-highway car and pedestrian accident rates in the presence of coastal flooding.

Accident rates versus travel time delays present differing pictures of traffic resilience for communities in the San Francisco Bay Area. One of the central results of Kasmalkar et al. Kasmalkar et al. (2020) is that communities with high road network density are resilient to flood-related delays, because they have sufficient alternate road capacity to offset road closures or unexpected increases in traffic volumes. As a result, southwestern communities, especially those around the city of San Jose that have dense road networks, have relatively low projected delays despite the flooding of segments of major highways such as the US-101 (Kasmalkar et al., 2020).

However, when cars on flooded highways are rerouted onto local roads that pass through residential communities, the potential increase in traffic volumes may cause spikes in car and pedestrian accident rates. Thus, the availability of alternate roads may reduce the road safety of communities by accommodating an increase in traffic volumes. Our results in Figs. 10 and 12 suggest large increases in accident rates with flooding in communities around the major cities of Napa, Oakland, San Francisco, San Jose and Santa Rosa, where road network density is relatively high. The increase in pedestrian accident rates is almost exclusively concentrated around the major cities – a consequence of the high pedestrian volumes within the cities (Lee and Abdel-Aty, 2005). The increase in accident rates with flooding is largest during peak-hour traffic because a relatively large number of peak-hour commuters are rerouted off of flooded highways. Accident rates do not increase to the same degree during non–peak hours because the disrupted traffic volumes are relatively small.

Flood-related changes in accident rates and travel times also differ at the regional level. Travel time delays increase with water level

in steps, where the delays are relatively low up to the 24–inch water level but are substantially higher for the 36–inch water level (Kasmalkar et al., 2020). The step-like behavior is likely related to the successive closures of key nexus points at specific water levels, causing substantial region-wide changes in traffic patterns (Kasmalkar et al., 2020). For example, the Dumbarton bridge, a major low-lying traffic corridor which runs across the Bay, remains open up to the 24–inch water level but is projected to be closed at the 36–inch water level. Upon closure, a large number of commuters are forced to travel either across a different bridge or along the entire southern shoreline of the Bay, causing substantial travel time delays at that water level (Kasmalkar et al., 2020).

Similar to delays, our study suggests that peak-hour (7–10 am) accident rates also increase with water level. However, the rate of increase diminishes with water level (Fig. 13). As a result, the largest increase in accident rates occurs when the water level increases from 0 to 12 in.. One potential reason for the greater increase in accident rates at low water levels is that rerouted traffic may already saturate the local roads of certain communities. Additional increase in water level may then only marginally increase the traffic volumes in the saturated communities while slowing down traffic instead, causing a negligible increase in accident rates. Additionally, at high water levels, the previously described region-wide changes in traffic patterns reroute commuters onto alternate traffic corridors, such as from the Dumbarton Bridge to the San Mateo Bridge, rather than onto local roads in the vicinity of their usual routes. As a result, traffic volumes on local roads and the corresponding accident rates tends to increase only minimally at high water levels.

Overall, the contrasting changes in accident rates and delays with water level suggest that, at low-to-moderate water levels, the risk of accidents may pose a similar, if not a greater concern than travel time delays for communities in the San Francisco Bay Area. The increase in projected accident rates for the 12–inch water level also demonstrates the immediacy of the problem. Coastal flood events building up to a water level of 12 in. are to be expected in the 2020–2040 period, even at the present-day sea level (Vandever et al., 2017). Particularly affected could be densely populated communities adjacent to major traffic corridors, such as the US-101 which lines the western shore of the inner San Francisco Bay and is only slightly elevated above sea level for wide stretches. The densely populated communities such as those in San Francisco City tend to have dense road networks, allowing for greater rerouting of traffic from potentially flooded highways to local roads, and a correspondingly greater increase in accident rates.

We emphasize that our estimates of accident rates for the San Francisco Bay Area under flooding conditions are computed from regressions between historical accident rates and modeled traffic volumes. The validity of our estimates is limited both by the applicability of historic data and by the validity of our modeled traffic volumes. The ability to work remotely and the advent of autonomous vehicles are just two factors which may alter the representativeness of historic data in estimating future accident rates. Similarly, our model introduces both aleatoric uncertainty (see Fig. 4), arising from the ill-constrained parameters relating travel times and traffic volumes (Kasmalkar et al., 2020; Erhardt et al., 2012; Branston, 1976; Miller and Baker, 2016; Kim and Mahmassani, 1987), and systematic uncertainty, arising from potential changes in commuter behavior in response to technological innovation.

Our traffic model applies only to an average commute and does not capture day-to-day variability in traffic volumes. Assuming average commutes, our model estimates the hourly trends in traffic volumes over the 5–10 am time period, which introduces time as a confounding factor in our analysis. For example, the increase in pedestrian accident rates during the 8–9 am time period relative to the 6–7 am time period may be a consequence of increased school-related pedestrian activity within that hour, rather than a result of increased traffic volumes. Also, adverse road conditions such as temporary construction work, special events, and even accidents themselves, may cause accidents. These dynamics are not considered here.

Despite the multiple uncertainties, we argue that the main value of our work lies in identifying the biases associated with quantifying traffic resilience primarily, or even exclusively, from an efficiency point of view as done in several previous studies (Kasmalkar et al., 2020; Ganin et al., 2017; Freckleton et al., 2012). It is important to keep in mind that the flood-related closure of highways displaces traffic into nearby residential communities, potentially elevating the risk of accidents in those communities. This dynamic is probably not unique to the San Francisco Bay Area, and could be relevant for other urban areas where some of the major traffic corridors are low-lying and prone to flooding.

7. Conclusion

This study quantifies the traffic resilience of communities to flood-related traffic disruption by estimating the increases in non-highway car and pedestrian accident rates as a result of traffic being displaced onto local roads. We use regression models to develop statistical relationships between traffic volumes and historical accident rates, and project accident rates for a range of water levels using simulated traffic patterns. Our study shows that the flooding of highways forces a large number of commuters onto local roads, thus increasing the accident rates for the nearby communities, especially during peak-hour traffic.

Our analysis shows that quantifying traffic resilience in terms of the rate of accidents rather travel time delays changes the classification of the relative resilience of communities in the San Francisco Bay Area. As sea level rises, delays increase in communities where the road network lacks sufficient alternate road capacity to offset flood-related traffic disruption. In contrast, accident rates increase the most around major cities, where the high availability of alternate roads brings in displaced traffic. Region-wide accident rates increase the most at low water levels, while delays increase sharply at higher water levels, suggesting that accidents may be a greater concern than delays at low-to-moderate water levels.

Funding

This research was funded by the UPS Endowment Fund for Transportation, Logistics, and Urban Issues, and Stanford's Bill Lane Center for the American West supported by the NSF through the Office of Polar Programs awards PLR-1744758 and PLR-1739027. We also acknowledge support from the following organizations that are part of, or affiliated with, Stanford University: the Haas Center for

Public Service; the School of Earth, Energy and Environmental Sciences; the Department of Civil and Environmental Engineering; the Institute for Computational and Mathematical Engineering; the Center for Sustainable Development and Global Competitiveness; and the Woods Institute for the Environment.

Data availability

The Python code for the traffic simulation model is available at http://cees-gitlab.stanford.edu/sigma/flood-related-traffic-disruption. The R code for the accident analysis is available at http://cees-gitlab.stanford.edu/sigma/2021-urban-climate-flood-related-accident-rates

Declaration of Competing Interest

The authors declare that they have no known competing financial interests or personal relationships that could have appeared to influence the work reported in this paper.

Acknowledgements

Our work is the product of the Stanford Future Bay Initiative, a research-education-practice partnership committed to co-production of actionable intelligence with San Francisco Bay Area communities, to shape a more equitable, resilient, and sustainable urban future. This research was motivated and shaped by stakeholder meetings with residents of North Fair Oaks, who highlighted local concerns around road safety. We thank Aditya Medury for insightful conversations regarding the development of accident models. We also thank Eric Dunham and Jack Baker for thoughtful comments on our work. We thank the University of California at Berkeley Transportation Injury Mapping System team for curating accident records into a query database. We also thank an anonymous reviewer for constructive comments.

Appendix A. Commuters by time of leaving for work

In Table A.1, we summarize the American Community Survey data (United States Census Bureau, 2017a) to specify the percentage of commuters in the San Francisco Bay Area who leave for work within a given time period. The percentages are used in our model to estimate the number of commuters during the morning hours.

Table A.1
Region-wide percentages of commuters by time of leaving for work. Values derived from ACS 2013–2017 survey data (United States Census Bureau, 2017a).

	5–6 am	6–7 am	7–8 am	8–9 am	9–10 am
Percentage of commuters leaving for work in this time period.	9%	18%	31%	28%	13%

Appendix B. Accidents by type and time of morning

In Table B.1, we summarize the region-wide accident counts in the San Francisco Bay Area for the 2013–2019 period by hour of occurrence and type, namely, highway, non-highway, or pedestrian. The data is obtained from the California Statewide Integrated Traffic Records System (California Highway Patrol, 2019).

Table B.1
Accidents in the San Francisco Bay Area by type and time period, curated from (California Highway Patrol, 2019).

Time Period	Accidents		
	Pedestrian	Non-highway Car	Highway Car
5–6 am	201	856	1523
6–7 am	449	1755	2349
7–8 am	900	4224	3433
8–9 am	1085	5688	3975
9–10 am	645	4229	2806
Total	**3,280**	**16,752**	**14,086**

Appendix C. Validation of modeled travel times

We present validation data in the form of histograms of the difference between TomTom and modeled travel times. The histograms

for the 6–7 am and 8–9 am time periods are shown in Fig. 2, while the histograms for the 5–6 am, 7–8 am, and 9–10 am are displayed in Fig. C.1. All 5 histograms show similar single-peak distributions that are skewed to the right, suggesting that our model tends to underestimate actual travel time. The deviations are not surprising, since our model does not incorporate external factors such as accidents or construction sites, all of which will tend to delay traffic.

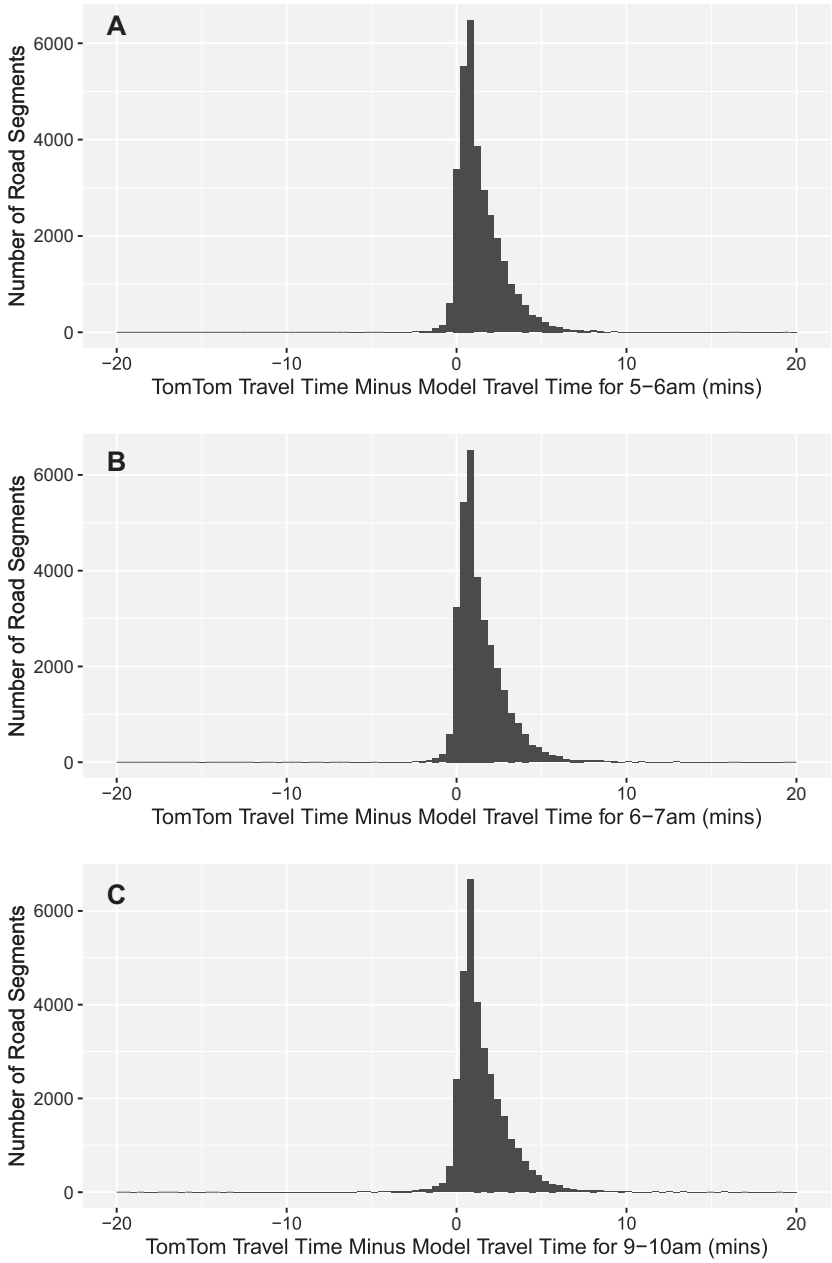

Fig. C.1. Histograms for differences in TomTom and modeled travel times over all segments in the model road network. Travel times differences for (a) 5–6 am, (b) 7–8 am, and (c) 9–10 am. The results are similar to Fig. 2.

Appendix D. Alternate partitions of San Francisco Bay Area

To test the degree to which clustering may alter the relationship between accident rates and traffic volumes that we infer, we consider two alternate clustering schemes in Fig. D.1 (car accidents) and Fig. D.2 (pedestrian accidents). The first scheme prioritizes the proximity of census blocks, while the second scheme prioritizes similar median household incomes and free flow travel speeds over proximity. Overall, the broad spatial similarities of Fig. D.1 to Fig. 6 and Fig. 8, respectively, suggests that the choice of the clustering approach may alter our results at the community scale but has limited impact on our results at larger spatial scales.

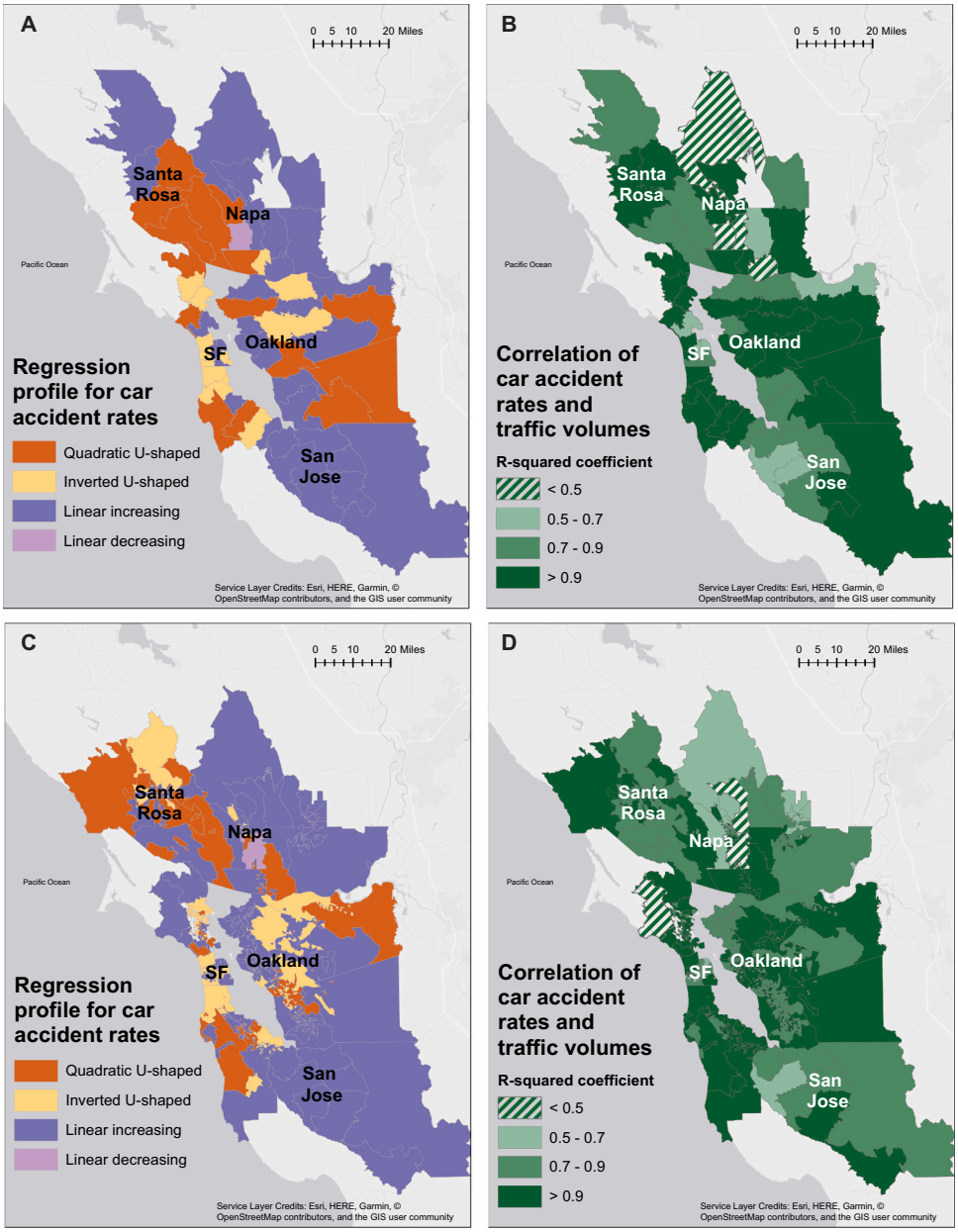

Fig. D.1. Spatial distribution of the regression curves for non-highway car accident rates and traffic volumes for alternate clusters of San Francisco Bay Area census blocks. The panels are organized similar to Fig. 6. Panels A and B represent a clustering which optimizes for proximity, while Panels C and D represents a clustering which optimizes for similarity of median household income and mean free flow travel speeds. In the latter, not all communities may be contiguous areas.

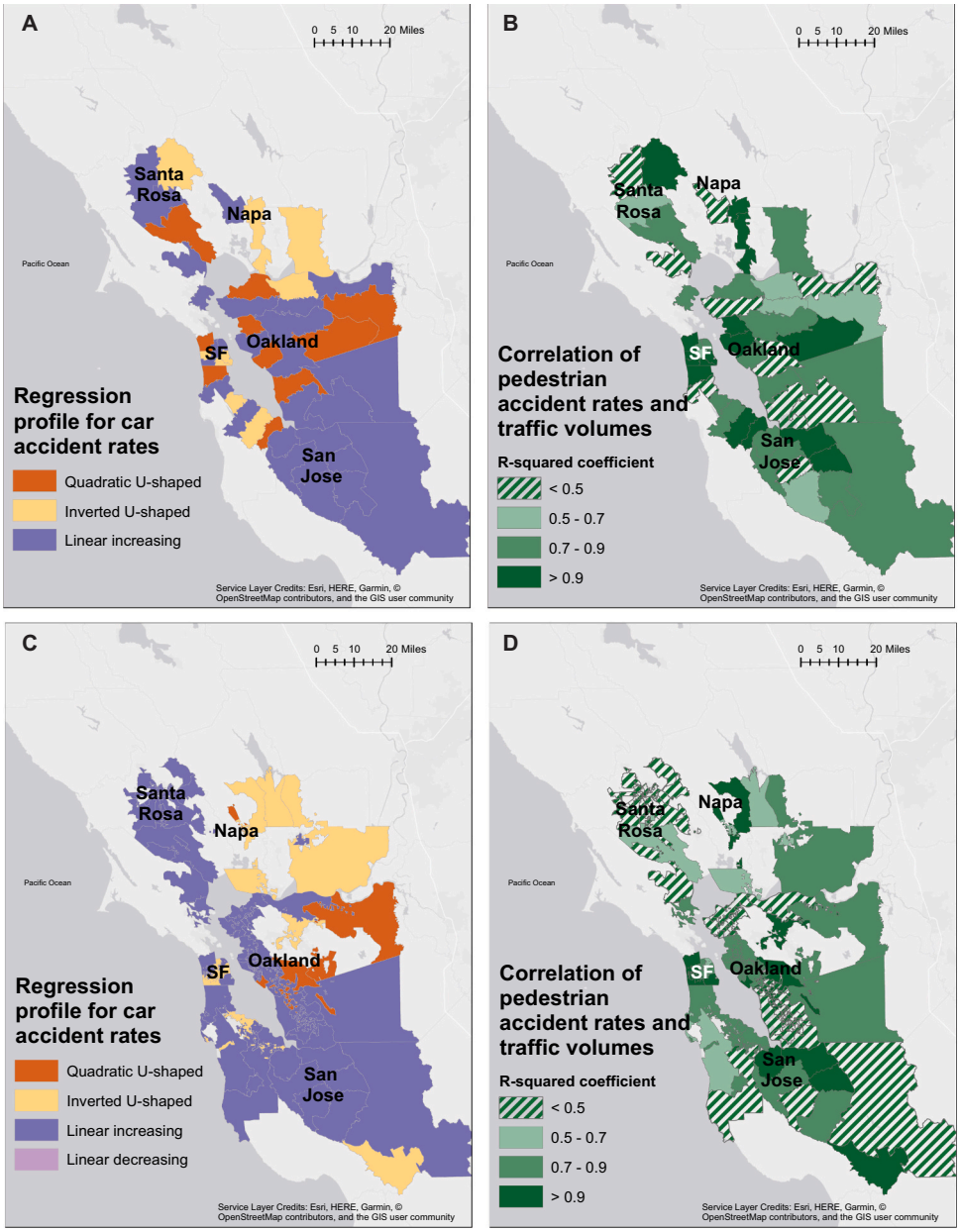

Fig. D.2. Spatial distribution of the regression curves for pedestrian accident rates and traffic volumes for alternate clusters of San Francisco Bay Area census blocks. The panels are organized similar to Fig. 6. Panels A and B represent a clustering which optimizes for proximity, while Panels C and D represents a clustering which optimizes for similarity of median household income and mean free flow travel speeds. In the latter, not all communities may be contiguous areas.

Appendix E. Accidents rates for the San Francisco Bay Area estimated purely from linear regression

We present estimates for accident rates in the presence of flooding using only linear regression. The results indicate that the overall spatial distribution of accident rates in the San Francisco Bay Area remains robust when limiting the analysis to linear regression.

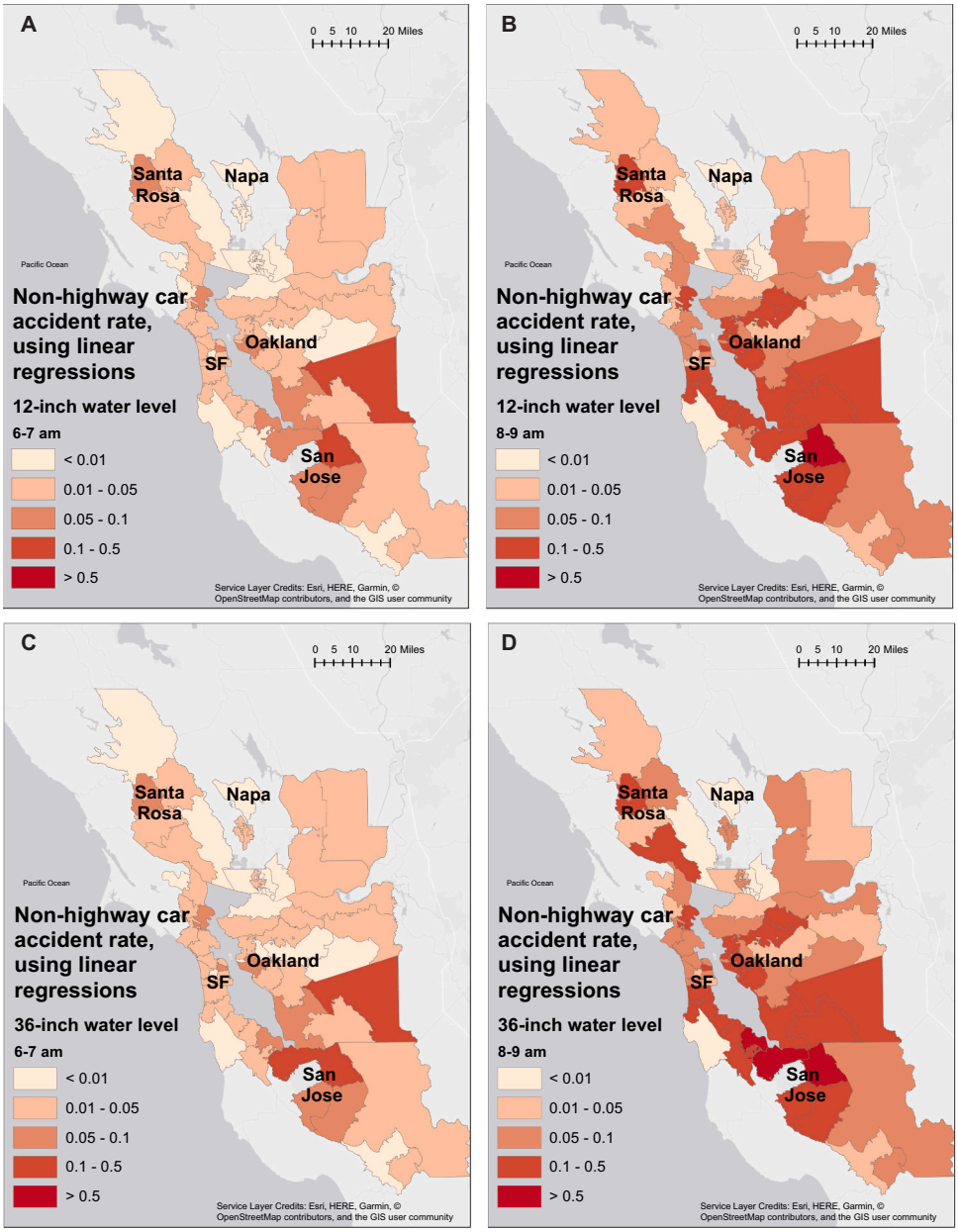

Fig. E.1. Model estimates of non-highway car accident rates with flooding, obtained purely from linear regressions. (A, B) 6–7 am and 8–9 am, respectively, for the 12–inch water level. (C, D) Same as (A, B), for the 36–inch water level. Communities with insufficient accident data and low R^2 regression coefficients are removed.

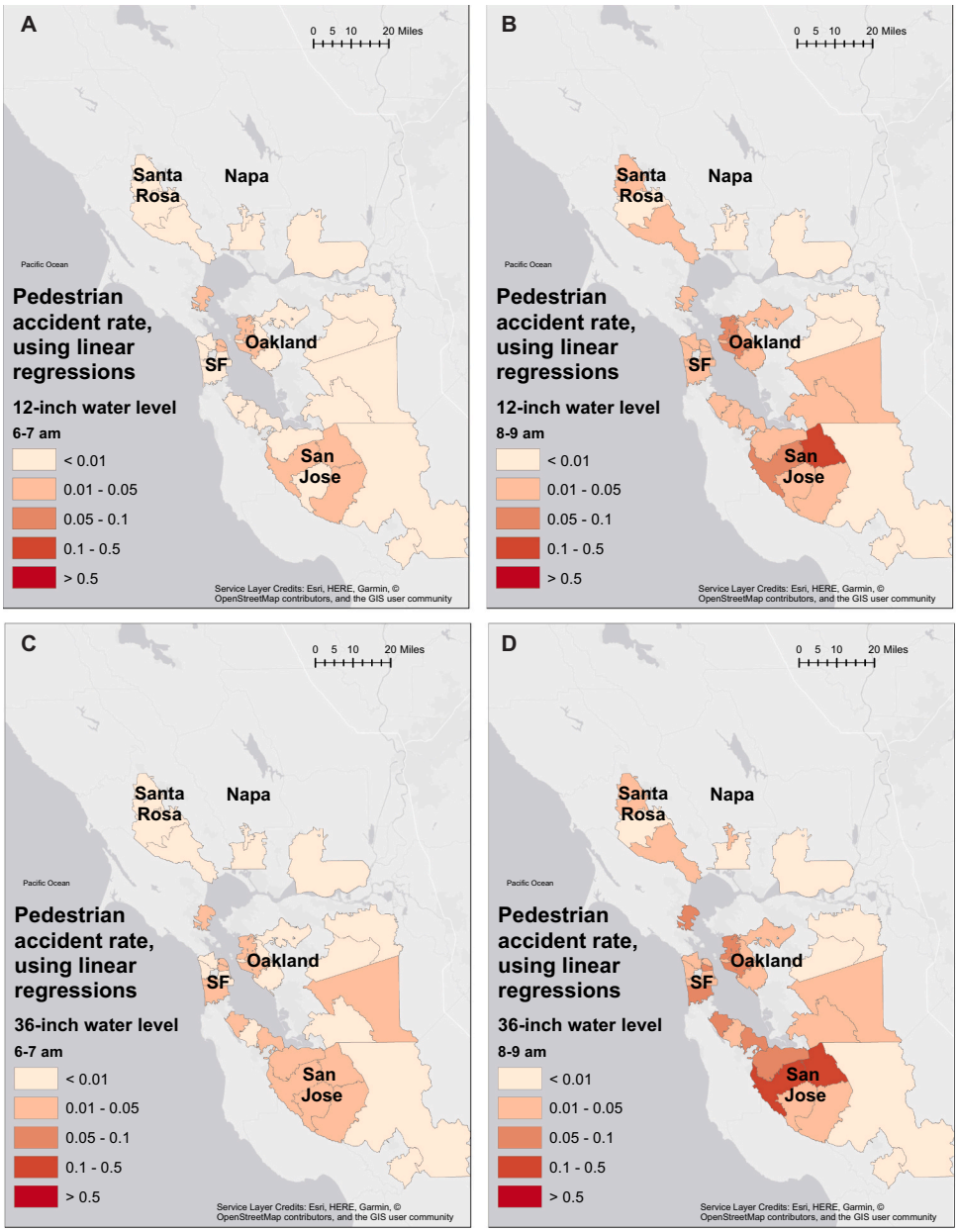

Fig. E.2. Model estimates of pedestrian accident rates with flooding, obtained purely from linear regressions. (A, B) 6–7 am and 8–9 am, respectively, for the 12–inch water level. (C, D) Same as (A, B), for the 36–inch water level. Communities with insufficient accident data and low R^2 regression coefficients are removed.

Appendix F. Validating the increase in accident rates with coastal water level

Our study projects that non-highway car and pedestrian accident rates increase with coastal water level in the San Francisco Bay Area. Our analysis further suggests that the increase in accident rates is caused by flood-related closures of major highways forcing commuters onto local roads passing through residential communities. Given that our results suggest an increase in accident rates on flood days under present and near-future conditions, the question arises whether there is any indication in existing data to tentatively support this claim.

In this Appendix, we test whether accident rates may have been higher on flood days in the recent past. To do that, we first compute the region-wide historical accident counts averaged for the peak hour 7–10 am time period for each weekday in the 2013–2019 period using the Statewide Integrated Traffic Records System (California Highway Patrol, 2019). We then use a monthly moving average to remove the temporal trend from the historical accident counts. Next, we join the historical accident data to the average reading of the

mean higher high water level for the 7–10 am time period from the San Francisco City tidal gauge (National Oceanic and Atmospheric Administration, 2018). Finally, we identify the days when the tidal gauge reading from the 7–10 am time period is greater than 12 in., and perform a statistical *Z*-test to check if the accident count during days of flooding is higher than the mean accident count.

There are a total of 7 flood days in the 2013–2019 period with water level greater than 12 in.. We present the detrended non-highway car accident count for the days with flooding in Table F.1. The average detrended accident count for the flood days for the 7–10 am time period is 0.28 accidents, while the average detrended accident count for all days is 0. The statistical Z-test highlights that achieving a detrended accident count of at least 0.28 accidents purely by normal random chance has *p*-value $P = 0.12$. The relatively small p-value suggests that, with moderate-to-high probability, the accident count on flood days is higher than on non-flood days.

Table F.1
Non-highway car accident counts averaged over the 7–10 am time period for days with mean higher high-water level greater than 12 in.. The accident rates are derived from (California Highway Patrol, 2019) and the water levels are derived from (National Oceanic and Atmospheric Administration, 2018).

Date	Water level (inches)	Accident count	Detrended count
2014-12-03	17	2	0.11
2015-12-22	14	2.3	−0.06
2016-01-05	13	1.7	−0.17
2016-01-19	13	2.7	0.83
2017-01-09	14	2	−0.27
2017-02-07	17	4.3	1.63
2019-01-17	15	2	−0.35
2019-02-14	13	3	0.52
Mean		2.5	0.28

The historical data for pedestrian accidents on flood days is shown in Table F.2. The pedestrian accident counts, averaged over the 7–10 am time period, are substantially smaller than the non-highway car accident rates in Table F.1. The detrended pedestrian accident counts also show a smaller increase, 0.01 accidents, than for detrended car accidents. The p-value for achieving the excess accident count over the average detrended accident count for all days is $P = 0.48$. The analysis suggests that there is almost a 50% chance that the marginally higher pedestrian accident counts on flood days are a result of pure randomness, indicating that the validation for the case of pedestrian accidents is less conclusive than for the case of car accidents.

Table F.2
Pedestrian accident counts averaged over the 7–10 am time period for days with mean higher high-water level greater than 12 in.. The accident rates are derived from (California Highway Patrol, 2019) and the water levels are derived from (National Oceanic and Atmospheric Administration, 2018).

Date	Water level (inches)	Accident count	Detrended count
2014-12-03	17	0.33	−0.27
2016-01-05	13	0.33	−0.42
2016-01-19	13	2	1.24
2017-01-09	14	0.33	−0.46
2017-02-07	17	0.67	0.05
2019-01-17	15	0.33	−0.18
2019-02-14	13	0.67	0.12
Mean		0.6	0.01

The accident counts in Tables F.1 and F.2 are smaller than the model outputs for any of the peak hours (7–10 am) in Fig. 13. Some of the potential reasons for the disparity are, the small sample ($n = 7$) of flood days recorded within the tidal gauge data; the lack of observed extreme water levels, particularly those exceeding 24 or 36 in.; and the use of a single tide gauge for obtaining water level data rather than combining a network of tidal gauges. Nevertheless, this preliminary statistical analysis is consistent with our model result that non-highway car accident counts during morning hours are relatively higher on flood days than on regular days, indicating a potential effect of coastal flooding on accident rates.

References

Branston, D., 1976. Link capacity functions: a review. Transp. Res. 10 (4), 223–236 issn: 00411647. https://doi.org/10.1016/0041-1647(76)90055-1.
Brodsky, H., Hakkert, A., 1988. Risk of a road accident in rainy weather. Accid. Anal. Prev. 20 (3), 161–176. ISSN: 0001-4575. https://doi.org/10.1016/0001-4575(88)90001-2.
Brüde, U., Larsson, J., Hedman, K.-O., 1998. Design of major urban junctions: accident prediction models and empirical comparisons. VTI EC Res. 3.
California Highway Patrol, 2019. Statewide Integrated Traffic Records System (SWITRS) - Dataset. URL: https://tims.berkeley.edu/.

Chen, M., Alfa, A.S., 1991. A network design algorithm using a stochastic incremental traffic assignment approach. Transp. Sci. 25 (3), 215–224 issn: 0041–1655. https://doi.org/10.1287/trsc.25.3.215.
Erhardt, G., Brinckerhoff, P., Ory, D., Sarvepalli, A., Freedman, J., Hood, J., Stabler, B., 2012. MTC's Travel Model One: Applications of an Activity-Based Model in its First Year. Tampa, Florida.
Falcocchio, J.C., Levinson, H.S., 2015. Road Traffic Congestion: A Concise Guide, vol. 7. Springer.
Freckleton, D., Heaslip, K., Louisell, W., Collura, J., 2012. Evaluation of resiliency of transportation networks after disasters. Transp. Res. Rec. 2284 (1), 109–116 issn: 0361–1981. https://doi.org/10.3141/2284-13.
Ganin, A.A., Kitsak, M., Marchese, D., Keisler, J.M., Seager, T., Linkov, I., 2017. Resilience and efficiency in transportation networks. Sci. Adv. 3 (12), e1701079 https://doi.org/10.1126/sciadv.1701079 url: http://advances.sciencemag.org/content/3/12/e1701079.abstract.
Gwynn, D., 1967. Relationship of accident rates and accident involvements with hourly volumes. Traffic Quart. 21 (3) (issn: 0041-0713).
Hummel, M.A., Wood, N.J., Schweikert, A., Stacey, M.T., Jones, J., Barnard, P.L., Erikson, L., 2018. Clusters of community exposure to coastal flooding hazards based on storm and sea level rise scenarios—implications for adaptation networks in the San Francisco Bay region. Reg. Environ. Chang. 18 (5), 1343–1355.
Kasmalkar, I.G., Serafin, K.A., Miao, Y., Bick, I.A., Ortolano, L., Ouyang, D., Suckale, J., Aug. 2020. When floods hit the road: Resilience to flood-related traffic disruption in the San Francisco Bay Area and beyond. Sci. Adv. 6 (32), eaba2423. ISSN: 2375-2548.
Kerner, B.S., 2012. The Physics of Traffic: Empirical Freeway Pattern Features, Engineering Applications, and Theory. Springer-Verlag Berlin Heidelburg, Tampa, Florida.
Kim, Y.G., Mahmassani, H.S., 1987. Link Performance Functions for Urban Freeways With Asymmetric Car-Truck Interactions, pp. 32–39.
Koetse, M.J., Rietveld, P., 2009. The impact of climate change and weather on transport: an overview of empirical findings. Transp. Res. Part D: Transp. Environ. 14 (3), 205–221. ISSN: 1361-9209.
Lee, C., Abdel-Aty, M., 2005. Comprehensive analysis of vehicle-pedestrian crashes at intersections in Florida. Accid. Anal. Prev. 37 (4), 775–786. ISSN: 00014575. https://doi.org/10.1016/j.aap.2005.03.019.
Lord, D., Mannering, F., 2010. The statistical analysis of crash-frequency data: a review and assessment of methodological alternatives. Transp. Res. Part A: Policy Pract. 44 (5), 291–305. ISSN: 09658564.
Martin, J.-L., 2002. Relationship between crash rate and hourly traffic flow on interurban motorways. Accid. Anal. Prev. 34 (5), 619–629.
Maycock, G., Hall, R.D., 1984. Accidents at 4-arm roundabouts. Tech. Rep. 249, 15–30.
Merkens, J.-L., Reimann, L., Hinkel, J., Vafeidis, A.T., 2016. Gridded population projections for the coastal zone under the shared socioeconomic pathways. Glob. Planet. Chang. 145, 57–66. ISSN: 0921-8181.
Metropolitan Transportation Commission/Association of Bay Area Governments (MTC/ABAG), 2017. Regional Road Network — Shapefile. URL: http://analytics.mtc.ca.gov/foswiki/bin/view/Main/DataRepository.
Miller, M., Baker, J.W., 2016. Coupling mode-destination accessibility with seismic risk assessment to identify at-risk communities. Reliab. Eng. Syst. Saf. 147, 60–71.
Mtoi, E.T., Moses, R., 2014. Calibration and evaluation of link congestion functions: applying intrinsic sensitivity of link speed as a practical consideration to heterogeneous facility types within urban network. J. Transp. Technol. 04 (02), 141–149 issn: 2160-0473. https://doi.org/10.4236/jtts.2014.42014.
National Oceanic, Atmospheric Administration, 2018. Turn Around Don't Drown. URL: https://www.weather.gov/safety/flood-turn-around-dont-drown.
Neumann, B., Vafeidis, A.T., Zimmermann, J., Nicholls, R.J., 2015. Future coastal population growth and exposure to sea-level rise and coastal flooding - a global assessment. PLoS One 10 (3), e0118571. https://doi.org/10.1371/journal.pone.0118571.
Pescaroli, G., Alexander, D., 2016. Critical infrastructure, panarchies and the vulnerability paths of cascading disasters. Nat. Hazards 82 (1), 175–192 issn: 1573–0840. https://doi.org/10.1007/s11069-016-2186-3.
Pregnolato, M., Ford, A., Wilkinson, S.M., Dawson, R.J., 2017. The impact of flooding on road transport: a depth-disruption function. Transport. Res. Part D: Transp. Environ. 55, 67–81 issn: 1361-9209. https://doi.org/10.1016/j.trd.2017.06.020.
Qiu, L., Nixon, W.A., 2008. Effects of adverse weather on traffic crashes: systematic review and meta-analysis. Transp. Res. Rec. 2055 (1), 139–146 issn: 0361–1981. https://doi.org/10.3141/2055-16.
Quddus, M.A., 2008. Modelling area-wide count outcomes with spatial correlation and heterogeneity: an analysis of London crash data. Accid. Anal. Prev. 40 (4), 1486–1497. ISSN: 0001-4575.
Raff, M.S., 1953. Interstate highway - accident study. Highway Res. Board Bull. 74, 18–45 issn: 0073–2206.
Retallack, A.E., Ostendorf, B., 2019. Current understanding of the effects of congestion on traffic accidents. Int. J. Environ. Res. Public Health 16 (18). https://doi.org/10.3390/ijerph16183400 issn: 1660–4601 (Electronic).
Retallack, A.E., Ostendorf, B., Feb. 2020. Relationship between traffic volume and accident frequency at intersections. Int. J. Environ. Res. Public Health 17 (4), 1393. ISSN: 1660-4601.
Suarez, P., Anderson, W., Mahal, V., Lakshmanan, T.R., May 2005. Impacts of flooding and climate change on urban transportation: A systemwide performance assessment of the Boston Metro Area. Transport. Res. Part D: Transp. Environ. 10 (3), 231–244 issn: 1361–9209. url: http://www.sciencedirect.com/science/article/pii/S1361920905000155.
TomTom, 2020. Routing API and Extended Routing API.
United Nations Population Division, 2018. World Urbanization Prospects: The 2018 Revision. Tech. Rep. United Nations Population Division.
United States Bureau of Public Roads, 1964. Traffic Assignment Manual for Application With a Large, High Speed Computer, vol. 2. United States Department of Transportation, Federal Highway Administration, Bureau of Public Roads.
United States Census Bureau, 2017a. American Community Survey 5-Year Estimates — Geodatabase: 2013–2017 Detailed Tables. URL: https://www.census.gov/geographies/mapping-files/time-series/geo/tiger-data.html.
United States Census Bureau, 2017b. Longitudinal Employer-Household Dynamics Origin Destination Employment Statistics — Geodatabase. URL: https://lehd.ces.census.gov/data/.
United States Census Bureau, 2018. TIGER/Line Shapefile, California, Census Blocks — Shapefile. URL: https://www.census.gov/geographies/mapping-files/time-series/geo/tiger-line-file.html.
Vandever, J., Lightner, M., Kassem, S., Guyenet, J., Mak, M., Bonham-Carter, C., 2017. Adapting to Rising Tides Bay Area Sea Level Rise Analysis and Mapping Project. URL: http://www.adaptingtorisingtides.org/wp-content/uploads/2018/07/BATA-ART-SLR-Analysis-and-Mapping-Report-Final-20170908.pdf.
Veh, A., 1937. Improvements to reduce traffic accidents. In: Meeting of the Highway Division: New York, NY, USA, pp. 1775–1785.
Wang, C., Quddus, M., Ison, S., 2013. A spatio-temporal analysis of the impact of congestion on traffic safety on major roads in the UK. Transport. A: Transp. Sci. 9 (2), 124–148.
Wang, P., Hunter, T., Bayen, A.M., Schechtner, K., González, M.C., 2012. Understanding road usage patterns in urban areas. Sci. Rep. 2, 1001. https://doi.org/10.1038/srep01001.
Wong, P.P., Losada, I.J., Gattuso, J.P., Hinkel, J., Khattabi, A., McInnes, K.L., Saito, Y., Sallenger, A., 2014. In: Field, C.B., Barros, V.R., Dokken, D.J., Mach, K.J., Mastrandrea, M.D., Bilir, T.E., White, L.L. (Eds.), Chapter 5. Coastal Systems and Low-lying Areas.
Wood, N.J., Jones, J., Spielman, S., Schmidtlein, M.C., Apr. 2015. Community clusters of tsunami vulnerability in the US Pacific northwest. Proceed. Nat. Acad. Sci. U. S. A. 112 (17), 5354–5359. ISSN: 10916490.
Xu, C., Wang, W., Liu, P., 2013. Identifying crash-prone traffic conditions under different weather on freeways. J. Saf. Res. 46, 135–144. ISSN: 0022-4375. https://doi.org/10.1016/j.jsr.2013.04.007. URL: http://www.sciencedirect.com/science/article/pii/S0022437513000510.